Grain size effects on Th-230(xs) inventories in opal-rich and carbonate-rich marine sediments

Grain size effects on $^{230}Th_{xs}$ inventories in opal-rich and carbonate-rich marine sediments

Sven Kretschmer[1, 2], Walter Geibert[3, 4], Michiel M. Rutgers van der Loeff[1], Gesine Mollenhauer[1, 2]

[1]Alfred Wegener Institute for Polar and Marine Research, Bremerhaven, Germany

[2]Universität Bremen, Fachbereich Geowissenschaften, Bremen, Germany

[3]School of GeoSciences, University of Edinburgh, UK

[4]Scottish Association for Marine Science, Dunstaffnage Marine Laboratory, Oban, UK

Corresponding author. Tel.: +49 421 218 65075; Fax: +49 471 4831 1425

E-mail address: sven.kretschmer@awi.de (S. Kretschmer)

Abstract

Excess Thorium-230 ($^{230}Th_{xs}$) as a constant flux tracer is an essential tool for paleoceanographic studies, but its limitations for flux normalization are still a matter of debate. In regions of rapid sediment accumulation, it has been an open question if $^{230}Th_{xs}$-normalized fluxes are biased by particle sorting effects during sediment redistribution. In order to study the sorting effect of sediment transport on $^{230}Th_{xs}$, we analyzed the specific activity of $^{230}Th_{xs}$ in different particle size classes of carbonate-rich sediments from the South East Atlantic, and of opal-rich sediments from the Atlantic sector of the Southern Ocean. At both sites, we compare the $^{230}Th_{xs}$ distribution in neighboring high vs. low accumulation settings. Two grain-size fractionation methods are explored.

We find that the $^{230}Th_{xs}$ distribution is strongly grain size dependent, and 50-90% of the total $^{230}Th_{xs}$ inventory is concentrated in fine material smaller than 10μm, which is preferentially deposited at the high accumulation sites. This leads to an overestimation of the focusing factor Ψ, and consequently to an underestimation of the vertical flux rate at such sites. The distribution of authigenic uranium indicates that fine organic-rich material has also been re-deposited from lateral sources. If the particle sorting effect is considered in the flux calculations, it reduces the estimated extent of sediment focusing. In order to assess the maximum effect of particle sorting on Ψ, we present an extreme scenario, in which we assume a lateral sediment supply of only fine material (<10μm). In this case, the focusing factor of the opal-rich core would be reduced from Ψ=5.9 to Ψ=3.2. In a more likely scenario, allowing silt-sized material to be transported, Ψ is reduced from 5.9 to 5.0 if particle sorting is taken into consideration. The bias introduced by particle sorting is most important for strongly focused sediments.

Comparing $^{230}Th_{xs}$-normalized mass fluxes biased by sorting effects with uncorrected mass fluxes, we suggest that $^{230}Th_{xs}$-normalization is still a valid tool to correct for lateral sediment

redistribution. However, differences in focusing factors between core locations have to be evaluated carefully, taking the grain size distributions into consideration.

Keywords

Thorium, sediment focusing, vertical flux, particle sorting, grain size distribution

1 Introduction

1.1 Main carrier phases for $^{230}Th_{xs}$ in water column and sediment

The accurate knowledge of vertical and lateral particle transport in the ocean is crucial for understanding the modern biogeochemical cycles and for paleoceanographic reconstructions. The naturally occurring radionuclide Thorium-230 (^{230}Th) is considered to be a powerful tracer of marine particle transport, because of its short residence time in the ocean and nearly constant flux to the seafloor (Henderson et al., 1999; Thomson et al., 1993). ^{230}Th is supplied to seawater uniformly at a rate of 0.0267dpm/m³/yr from decaying Uranium-234 (^{234}U). However, concentrations of dissolved ^{230}Th in seawater are very low because it becomes rapidly attached to suspended and sinking particles (=excess ^{230}Th, $^{230}Th_{xs}$) by the "reversible scavenging" mechanism (Bacon and Anderson, 1982; Nozaki et al., 1981). This process eventually transports ^{230}Th to the sea floor. Th sorption kinetics have been studied in vitro under well defined experimental conditions (e.g. Geibert and Usbeck, 2004; Guo et al., 2002) but results from in situ measurements (sediment traps or in situ-pumps) are difficult to interpret, leading to an on-going debate about the main carrier phases of adsorbed Th under natural conditions. In general, Th sorption in seawater has been found to be weak on biogenic silica (Chase et al., 2002; Roy-Barman et al., 2005). Main carrier phases have been identified as lithogenics (Luo and Ku, 1999), carbonates and lithogenics (Chase et al., 2002; Siddall et al., 2005), or Mn oxides (Roy-Barman et al., 2005; Roy-Barman et al., 2009). In the upper water column, findings of ^{234}Th (Santschi et al., 2006) suggest that most Th is transported by organic phases like acid polysaccharides, which are not likely to be transported unmodified to the sea floor.

Carrier phases can be classified by their composition and origin, or by different grain size fractions. As summarized by Rutgers van der Loeff and Geibert (2008), adsorbed Th can change the carrier phase during settling through the water column by numerous processes.

Once buried in the sediment, Th carrier phases are affected by early diagenetic processes, and also by lateral redistribution, e.g. in a nepheloid layer (Rutgers van der Loeff et al., 2002). Scholten et al. (1994) suggested restricting the application of $^{230}Th_{xs}$ normalized fluxes to those settings where the origin and grain-size dependent composition of focused sediment is known, a suggestion that has so far not been realized. When the $^{230}Th_{xs}$ normalization method was established, Bacon (1984) already recommended considering separately the fine and coarse fractions of carbonate sediments. François et al. (2004) advise that $^{230}Th_{xs}$ normalization should not be applied to the coarse fraction of the sediment as it is much less prone to lateral redistribution. However, to our knowledge, the grain size dependent distribution of ^{230}Th in sediments has been addressed in only three studies (Luo and Ku, 1999; Scholten et al., 1994; Thomson et al., 1993).

1.2 $^{230}Th_{xs}$ applications, assumptions and uncertainties

Using $^{230}Th_{xs}$ in sediments, we are able to distinguish between (a) vertical rain rate, providing the amount of sediment that settled vertically through the water column and (b) syndepositional or postdepositional sediment dislocation by currents, estimated with the focusing factor (Ψ) that characterizes sediment winnowing ($\Psi<1$) or focusing ($\Psi>1$) conditions. The method of $^{230}Th_{xs}$ normalization was developed by e.g. Bacon (1984), Suman and Bacon (1989) and François et al. (1990). It was reviewed by Frank et al. (1999), Henderson and Anderson (2003) and François et al. (2004).

Paleoceanographic studies often target locations of high sediment accumulation in order to achieve high temporal resolution. However, these locations are often strongly affected by lateral sediment redistribution (e.g. Bianchi and McCave, 2000; Ohkouchi et al., 2002) so that the reconstruction of the vertical particle fluxes needs to be corrected by $^{230}Th_{xs}$-normalization. Evidence for strong lateral redistribution has been detected e.g. in sediments from Bermuda Rise (Ψ13.2; Suman and Bacon, 1989), the Southern Ocean Indian sector

(Ψ12.5; François et al., 1993 and Ψ10.0; Dezileau et al., 2000), in the Southern Ocean Atlantic sector (Ψ7.7; Frank et al., 2000), in the equatorial Pacific (Ψ4; Marcantonio et al., 2001; Ψ8; Loubere et al., 2004 and Ψ7.5; Kienast et al., 2007). It is still unclear to which extent the corrected fluxes are biased due to particle sorting effects during sediment redistribution. This is an important aspect in recent discussions about the validity of the entire approach, e.g. in the equatorial Pacific (Broecker, 2008; François et al., 2007; Lyle et al., 2005, 2007; Thomas et al., 2000).

The main assumption for applying $^{230}Th_{xs}$ normalization and the focusing factor is that redistribution affects the total sediment, i.e. grains of all particle sizes are resuspended, transported and redeposited together. It is further assumed that sediment from the vertical flux and laterally supplied sediments are equal in composition, size distribution and $^{230}Th_{xs}$ concentration. In this study, we test the hypothesis that the grain size fractions differ in composition and $^{230}Th_{xs}$ activity. A further hypothesis is that the redistribution of particles is variable for different grain sizes and will introduce a sorting effect on $^{230}Th_{xs}$ inventories in sediments. For this purpose, we will (a) present data of $^{230}Th_{xs}$ distribution by sediment particle class and identify the main carrier phase, taking into consideration the effect of lithology (carbonate-rich vs. opal-rich), (b) compare $^{230}Th_{xs}$ inventories of rapidly and slowly accumulated sediments ("twin cores") and (c) calculate the maximum bias on the focusing factor introduced by the particle sorting effect.

2 Material and Methods

2.1 Sample selection

To study the influence of sediment redistribution on the $^{230}Th_{xs}$-signal, inventories of $^{230}Th_{xs}$ from neighboring sites, characterized by contrasting accumulation conditions, were compared. Therefore, two sediment cores ("twin cores") were chosen being in close vicinity to each other and similar in water depth. In addition, the stratigraphy needed to be well

constrained. We selected a twin core location fulfilling all requirements located in the Southern Ocean (PS1768-8 and PS1769-1). Because of its high content of biogenic silica this sediment is from hereon referred to as the "siliceous sediment". A second set of twin cores is located in the SE Atlantic Ocean (GeoB1027-2 and GeoB1028-4). We refer to it as "carbonate sediment" due to high content of $CaCO_3$. In the following, the two locations of the twin cores are described briefly.

2.1.1 Carbonate sediment

Two giant box corers, GeoB1027-2 and GeoB1028-4 were recovered at approximately 20°S, 9°E from the Walvis Ridge, South East Atlantic in the Benguela upwelling area with a lateral distance of 49km between core sites. GeoB1027-2 was taken in 2668m water depth, where an echosounder survey indicated focusing of surface sediment layers. In contrast, site GeoB1028-4 was collected from a depth 453m shallower, and less affected by focusing. The sediment of both core sites consisted of foraminiferal sand and carbonaceous mud. Near surface samples were taken from GeoB1027-2 at 13-16cm (3.1kyr) and from GeoB1028-4 at 16-19cm (4.8kyr) (Table 1).

2.1.2 Siliceous sediment

The second study area is located in the Southern Ocean, currently south of the Antarctic Polar Front and north of Bouvet Island in the permanently sea-ice-free Antarctic Zone. The gravity cores PS1768-8 and PS1769-1 were recovered at 52.6°S and 4.5°E with a lateral distance of 2.5km, in water depths of 3300m and 3270m, respectively. The Parasound survey revealed twofold higher sedimentation rates at site PS1768-8 than at the 30m shallower site PS1769-1. The sediment consisted of alternating layers of diatomaceous mud and ash-bearing diatomaceous mud with few calcareous microfossils (Gersonde and Hempel, 1990). Age control of sediment core PS1768-8 was established by radiocarbon dating and diatom stratigraphy. This core has been studied extensively (e.g. Diekmann et al., 2003;

Nürnberg et al., 1997; Zielinski et al., 1998). Frank et al. (1996) reported for this core site during Holocene and LGM a focusing factor of 4.5-6 and vertical rain rates of 1-4g/cm²/kyr. Sediment core PS1769-1 has been less extensively analyzed, and the stratigraphy was obtained by correlation of the magnetic susceptibility record with that of the parallel core PS1768-8. Samples were taken from core depths 1.66-1.69m (PS1768-8) and 0.14-0.16m (PS1769-1) with an interpolated age of 16 kyr (Table 1).

2.2 Grain size fractionation

In the following section we present two methods of sediment fractionation by sieving and settling in (a) purified water with ultrasonication and (b) natural seawater without ultrasonication. In most previous studies for grain size specific metal analysis the water used for wet sieving was discarded afterwards (e.g. Ackermann et al., 1983; Barbanti and Bothner, 1993; Koopmann and Prange, 1991). Förstner (2004) pointed out that generally wet sieving does not alter metal concentrations. However, the potential leakage of U and Th from solids to supernatant during the processing must be taken into account, which was one important consideration in this study.

2.2.1 Grain size fractionation in purified water

Samples were not dried prior to grain size fractionation in order to avoid artifacts by particle aggregation. The dry net weight was calculated using moisture content data determined separately. For desalination, samples were suspended in purified water (>15MΩ, Elix 5™, Millipore Corporation) (weight:volume 1:5) and agitated for two minutes, then centrifuged and decanted. This "washing" procedure was repeated three times for leaching the sea salt ions from the sediment because particles smaller than 10-20µm are prone to be coagulated by cations (Köster, 1964; McCave et al., 1995). For disaggregation, the samples were ultrasonicated. Chemical dispersants were not applied as these may interact with the particles' active surface layer and may affect Th adsorption. Samples were wet-sieved

subsequently with three nylon sieves (125µm, 63µm, 20µm) using purified water ("pureW") for 10min each. The particle suspension that passed the <20µm sieve was collected in cylinders for further fractionation into classes <2µm and 2-20µm based on the settling velocity principle. The terminal fall velocity of particles in an aqueous fluid was determined according to Stokes's law (descriptions e.g. in Köster, 1964 and Syvitski et al., 1991) assuming the particle density to be equal to the density of quartz (2.65g/cm³). The resulting grain sizes are quartz-equivalent spherical sedimentation diameters (ESSD). After a certain settling time, the fine fraction (ESSD: <2µm) remaining in suspension was siphoned off, while the coarser fraction (ESSD: 2-20µm) settled out from suspension to the bottom of the settling tube and was again resuspended in purified water. This procedure was repeated 10-20 times until the supernatant fluid achieved a low turbidity. Due to the repeated decantations the <2µm-fraction was recovered in a volume of 10 to 30L of water. As flocculation reagent, a $CaCl_2$-solution was added for extracting all particles from the water. The flocculated particles were allowed to settle down for four days, and then supernatant was decanted and stored separately in a canister.

The coarse fractions (>20µm) of the siliceous samples (PS1768 and PS1769) consisted of a mixture of biogenic opal particles and lithogenic particles that are distinctly different in densities (diatoms: ~1.1g/cm³ reported for different diatom species by van Ierland and Peperzak, 1984; quartz: 2.65g/cm³, Klein et al., 1985), which influence their hydrodynamic properties and hence their sinking velocity in a natural marine system. Therefore, a further separation by settling was performed. The three sieve fractions 20-63µm, 63-125µm and >125µm were split into slowly settling and fast settling fractions. Three settling velocities were specified: the maximum terminal velocity, $V_{t\text{-}max}$ (fast sinking particles), the minimum terminal velocity $V_{t\text{-}min}$ (slowly sinking particles) and the cut-off velocity V_c. $V_{t\text{-}max}$ was estimated assuming the average density of quartz (2.65g/cm³). $V_{t\text{-}min}$ was determined

empirically by measuring settling times of the slowest particles. V_c is the intermediate velocity between $V_{t\text{-}max}$ and $V_{t\text{-}min}$ that was chosen to siphon off the slowly settling fraction after the fast fraction settled to the bottom. This separation was repeated for each fraction 15-20 times until the supernatant fluid appeared clear.

The carbonate samples (GeoB1027 and GeoB1028) displayed homogeneous particle densities because this sediment was mainly composed of carbonaceous microfossils. For this reason the above described separation of slowly and fast settling was not applied to these samples.

2.2.2 Grain size fractionation in natural seawater

As we wanted to infer information about the transport of adsorbed particulate Th in seawater, we applied a second fractionation method with modified pretreatment and natural seawater as sieving fluid. The seawater technique should simulate "near-natural" conditions. Natural seawater ("seaW") was filtered through polycarbonate-filters (pore size 1µm) before sieving. The samples were suspended in seawater and agitated for 2 minutes. The sieve and settle process was as described in section 2.2.1, but omitting the desalination and ultrasonication steps. The separation into the classes <2µm and 2-20µm was not possible, as the smallest particles flocculated in seawater. Therefore the size class <20µm was split into <10µm and 10-20µm by settling as described in 2.2.1.

2.2.3 Processing of supernatants

In order to minimize the loss of Th and U by desorption effects, processing time was kept as short as possible, and small water volumes were used. However, assuming a leaching of U and Th due to desorption and dissolution effects, we collected the supernatant fluid (10-30L/sample) in canisters for further processing. First the supernatant was filtered through a polycarbonate-filter (1µm) in order to remove any remaining particulate Th. Moore and Hunter (1985) reported that 90-95% of particulate Th suspended in seawater is filtered by a

1.2µm-filter. The filter was fully digested and analyzed for Th and U isotopes following the same protocol for sediment analysis (section 2.3). The results of particulate Th and U on filters were not reported separately. Instead, they were included in the smallest fraction (<2µm or <10µm). The filtrated supernatant fluid was then acidified to pH 2-3 by addition of HNO_3 (subboiling distilled). A solution of iron chloride ($FeCl_3$ in HCl, 50mg/mL) was added together with the spikes ^{229}Th and ^{236}U. After 24 hours of equilibration, the pH was readjusted to pH 8 to 9 by adding NH_3 (suprapur®) for the co-precipitation with $Fe(OH)_3$ (Rutgers van der Loeff and Moore, 1999). The $Fe(OH)_3$-precipitate was re-dissolved in HNO_3, and Fe, Th and U were separated by ion exchange columns following the same protocol as described for the sediment samples (section 2.3).

2.2.4 Procedural blanks

Procedural blanks have been determined for both fractionation methods for comparison with the supernatants´ Th and U contents for detecting any potential loss or uptake of Th and U that occurred during the fractionation procedures. Two blanks were performed with purified water (8L each), and two blanks with seawater (5L and 22L). The procedural blanks accounted for 0.01-0.08% (^{230}Th), 0.01-0.15% (^{232}Th), 0.01-0.27% (^{238}U in pureW), and 70-200% (^{238}U in seaW) of the concentrations found in sediment samples.

2.3 Analysis of U and Th isotopes

Th and U isotopes were analyzed on freeze-dried samples (5-50mg) by isotope dilution, i.e. adding spikes of ^{229}Th (9pg) and ^{236}U (800pg) as internal standards. Samples and spikes were weighed into Teflon vials and fully dissolved in HNO_3 (3mL, concentrated, subboiling distilled), HCl (2mL, 30%, suprapur®) and HF (0.5mL, 40%, suprapur®) by heating to 225°C for 2h in a pressure-assisted microwave digestion system (CEM MARSXpress®). After sample digestion, the acid was fumed off until dry by gentle heating in the microwave evaporation system (CEM XpressVap®). The samples were then re-dissolved

in diluted HNO_3 (5mL, 1M, subboiling distilled) and heated to 150°C for 15min. Iron chloride (100µL) for precipitation was added. The $Fe(OH)_3$-precipitates of sediment samples and supernatant samples were re-dissolved in HNO_3 (3mL, 3M), and Fe, Th and U were separated by ion exchange with UTEVA® resin columns. Prior to separation, an $Al(NO_3)_3$ solution (150µL, 1M) was added to avoid unfavorable matrix interactions with, e.g., phosphate (Horwitz et al., 1993). The columns were conditioned with three column volumes (cv) HNO_3 (3M), then loaded with the samples and rinsed with HNO_3 (3cv 3M) for eluting Fe. Th was eluted with HCl (1cv 9M and 2cv 5M, suprapur®) followed by elution of U with HCl (3cv 0.02M). The eluates of U and Th were collected in Teflon beakers, evaporated, and re-dissolved in HNO_3 twice. U and Th fractions were diluted in 5mL HNO_3 (1M) and analyzed by Inductively Coupled Plasma-Sector Field Mass Spectrometry (ICP-SFMS, Element2, Thermo Scientific) with a desolvation system (Apex Q®, ESI). For details of machine settings see Martínez-Garcia et al. (2009). Within each batch of 24 samples, 2 replicates of the certified reference material (CRM) *UREM 11* and 2 procedural blanks were processed. The recommended value for the Uranium concentration in *UREM 11* is 58.9±0.5ppm (1σ; Hansen and Ring, 1983). From this value, we deduced the concentrations of the isotopes ^{238}U (58.5±0.5ppm) and ^{230}Th (957±8pg/g). The external reproducibility from replicate analyses (n=23) was within 3.8% for ^{238}U (60.4±2.3ppm) and 5.0% for ^{230}Th (959±48pg/g). The mean values in procedural blanks (n=21) were 253pg ^{238}U and 0.024pg ^{230}Th accounting for ~0.02% and ~0.6% of the samples, respectively. The results of Th and U specific activities in grain size fractions are given in dpm g^{-1} (disintegration per minute per gram of size fractionated particles).

2.4 Characterization of grain size fractions

Sediment fractions (seaW-method) of the samples GeoB1027-2 and PS1769-1 were examined in more detail by scanning electron microscopy (SEM), and their specific surface

area (SSA) was studied together with the grain size distribution (GSD) in order to further describe the result of particle separation. For the SEM study, sediment fractions were fixed on a sample holder, coated with gold and viewed with the SEM *XL30 Esem* (Philips) at 10.0kV.

The SSA was determined by gas adsorption analysis on a Quantachrome *Nova 2200*. The sediment samples were degassed and heated (110°C for 2h) to remove surface adsorbed water. After evacuation, the sediment was subjected to five partial pressures of N_2 gas (purity 99.996%) and the surface area was calculated using the BET-theory (Brunauer et al., 1938) according to ISO 9277.

Prior to the measurement of GSD, the dry sediment fractions were soaked in deionized water over night, sodium pyrophosphate ($Na_4P_2O_7$) was added, and the suspension was heated until boiling. We refrained from the removal of organic matter, carbonate and opal, as these components are assumed to be important carriers of particulate Th and U. The GSDs were determined with the *LS 13320 Laser Diffraction Particle Size Analyzer* (Beckman Coulter) in demineralized and degassed water.

The chemical composition (biogenic opal and some major elements) has been determined on the sediment fractions (seaW) of the samples PS1768-8 and PS1769-1. The determination of opal followed the description of Müller and Schneider (1993) where opal was extracted with NaOH (1 M) at 85°C, and dissolved silica was continuously analyzed by molybdate-blue spectrophotometry. The elements Mg, Al, K, Ca, Mn, Fe, Rb, and Cs has been analyzed on the samples after full acid digestion (see description for microwave digestion, section 2.3) using the ICP-SFMS Element2 (Thermo Scientific). Calibrations were done with certified standard solutions and external reproducibility was monitored using the NIST standard reference material 2702 (inorganics in marine sediment).

2.5 $^{230}Th_{xs}$ normalization and focusing factor

For particle flux studies, only the unsupported ^{230}Th deriving from scavenging (excess ^{230}Th) is of interest. For calculation of excess ^{230}Th activity, any ^{230}Th supported by detrital or authigenic U needs to be subtracted. The excess ^{230}Th activity then needs to be decay corrected (half-life 75380 years) to get the initial activity of excess ^{230}Th at the time of deposition (in the following referred to as $^{230}Th_{xs}$). $^{230}Th_{xs}$ is calculated following the descriptions of François et al. (2004) and Henderson and Anderson (2003). Briefly, the activity of $^{230}Th_{detrital}$ in lithogenic material (in secular equilibrium with $^{238}U_{detrital}$), and the activity of $^{230}Th_{authigen}$ derived from authigenic ^{234}U must be subtracted from the measured ^{230}Th activity. The activity of $^{238}U_{detrital}$ is inferred from the activity ratio $^{238}U/^{232}Th$ that has been suggested to be on average 0.6±0.1 for the Atlantic basin. The activity of $^{230}Th_{authigen}$ is estimated from authigenic ^{238}U (= $^{238}U_{total}$ - $^{238}U_{detrital}$), multiplied by 1.14 (activity ratio of $^{234}U/^{238}U$ in seawater), calculating the ^{230}Th production since the time of deposition. These calculations are based on assumptions for bulk samples and may be problematic for grain size separated samples, because size fractionation may produce a U/Th fractionation due to lithogenic minerals of different size classes. Especially the detrital $^{238}U/^{232}Th$ ratio could deviate significantly from the average value 0.6±0.1.

Following the assumption that ^{230}Th in seawater is completely scavenged and buried at the seafloor, $^{230}Th_{xs}$ specific activity in sediment is inversely related to the vertical flux of particles. According to Suman and Bacon (1989), the $^{230}Th_{xs}$ normalized sediment flux F_V is the vertical flux of any sediment constituent *i*, given by its ratio to the decay-corrected $^{230}Th_{xs}$. F_V is calculated by

$$F_V = \beta_{230} \times z \times f_i / [^{230}Th_{xs}],$$

where β_{230} is the annual production of ^{230}Th in the seawater (0.0267dpm m^{-3} yr^{-1}), z is the water depth (m), f_i is the weight fraction of component *i*, and $[^{230}Th_{xs}]$ is the specific activity of ^{230}Th [dpm g^{-1}] in the sediment at the time of deposition in excess of ^{234}U.

The focusing factor Ψ is given by the inventory of $^{230}Th_{xs}$ in the sediment section divided by the ^{230}Th production in seawater:

$$\Psi = [^{230}Th_{xs}] \times \rho \times (s_1 - s_2) / \beta_{230} \times z \times (t_1 - t_2),$$

where ρ is the mean dry bulk density (g cm^{-3}), s_1 and s_2 are the sediment depths (cm), and t_1 and t_2 are the corresponding ages (kyr).

3 Results

3.1 Recoveries of sediment, U and Th

The recoveries of sediment after the fractionation process range between 81% and 100% (Table 2). Recoveries of Th and U isotopes are 82-106% and 59-123%, respectively. The error propagation by summation of all grain size specific activities of a sediment sample yields errors of up to 12%, so that recoveries between 88% and 112% are generally regarded to be within the propagated error. Recoveries lower than 88% are probably due to loss of material. In contrast the high U recovery of sample PS1769-1 (seaW, 123%) could be possibly a result of U uptake from the natural seawater during fractionation processing. However, by comparing the U content in the procedural blanks with that in the supernatants, an enrichment of U in the supernatant has been detected that indicates an U loss from the sediment by leaching (28% of total sediment U is leached, Table 2). This discrepancy in sample PS1769-1 between high recovery of U and loss to supernatant remains an unexplained inconsistency. Leaching losses of ^{230}Th and ^{232}Th are low (0.3-3.9% and 0.5-2.2%, respectively). Due to the rather high losses of U to the processing water, the $^{230}Th_{xs}$ data of each grain size fraction may be undercorrected. Assuming that U leaching only affects the authigenic U (U_{auth}), and regarding the relatively young age of the samples, the contribution from decaying $^{234}U_{auth}$ to supported ^{230}Th is rather low. When the dissolved $^{234}U_{auth}$ fraction is included in ^{230}Th correction, $^{230}Th_{xs}$ results are reduced insignificantly by 0.02-0.45% (carbonate fractions), 0.001-0.41% (siliceous fractions >20µm) and 0.03-2.53% (siliceous

fractions <20µm). However, it is not possible to allocate the amount of dissolved U in the supernatant to any of the individual grain size fractions. Thus, the approximate errors introduced by U dissolution are included in the propagated errors calculated for the $^{230}Th_{xs}$ activity in each of the grain-size sediment fractions.

3.2 Fractionations with seawater versus purified water

The seaW fractionation produces grain size spectra that are overall coarser than the pureW-fractionation (Figure 1 & Figure 2). For example, at GeoB1027, the fraction <63µm accounts for 60% of the total sample when sieved with the seaW-method, but 79% using the pureW-method. Virtually all size classes >20µm contain higher specific activities of $^{230}Th_{xs}$ ^{232}Th and ^{238}U in the seaW-fractionated samples compared with the pureW-fractionation. The small particles <20µm contribute higher portions of $^{230}Th_{xs}$, ^{232}Th, and ^{238}U to the bulk sediment's inventory when fractionated with pureW (Table 3).

3.3 Distribution of fine sediment, Th and U at rapid versus slow accumulation sites

The isotopic composition of the carbonate sediment is dominated by the smallest particle class <2µm. This class accounts for 35-40 weight-% of the total sediment and it holds roughly 50-60% of the total sediment's Th and 30-60% of the total sediment's U (Table 3). The rapidly accumulated sediment (GeoB1027) is finer in grain size distribution. In contrast, the slowly accumulating sediment (GeoB1028) contains a much higher percentage of sand sized particles >125µm (36-42%). This leads to a remarkably high contribution to total Th (13-25%) and total U (31-41%) by the coarsest fraction at GeoB1028. The twin cores display identical $^{230}Th_{xs}$ activities within the smallest particles (<2µm and <10µm) (Figure 1). This is not the case for all particle classes coarser than 2µm (10µm), as they all display slightly but insignificantly higher $^{230}Th_{xs}$ activities at the rapidly accumulated core (GeoB1027).

The isotopic composition of the siliceous sediment is controlled by the smallest particle class <2µm, accounting for 40 weight-% of the total sediment, 60-70% of total ^{238}U,

70% of total ^{232}Th and 80-90% of total $^{230}Th_{xs}$ (Table 3). The deposition of fine particles <20µm is slightly higher at the rapidly accumulated core site (PS1768), and therefore it contributes more to the Th and U inventory than at the slowly accumulated core site (PS1769). The twin cores display identical $^{230}Th_{xs}$ activities within the smallest particles (<2µm and <10µm; Figure 2). The coarser particles (classes 10-20µm and fast sinking >20µm) are slightly but insignificantly higher in $^{230}Th_{xs}$ at the slow accumulation site (PS1769). ^{238}U activities in siliceous and carbonate sediments (Figure 1 and 2) reveal a regular distribution pattern for all grain sizes at both accumulation settings. The smaller the particles, the higher the U activities are, but with an overall lower level of U activity in the slowly accumulated sediment.

In the siliceous sediment, all fractions >20µm play a minor role as carrier for $^{230}Th_{xs}$, ^{232}Th, and ^{238}U (Figure 2; Table 3). In contrast, $^{230}Th_{xs}$, ^{232}Th, and ^{238}U in the carbonate sediment are more uniformly distributed between fine and coarse particles (Figure 1; Table 3), revealing a lower grain size effect than in the siliceous sediment, i.e., carbonate sand and coarse silt play an important role for Th and U inventories in carbonate sediments.

The scatter diagram (Figure 3) shows $^{230}Th_{xs}$ and ^{232}Th data from both carbonate and siliceous sediment fractions. On a linear regression line (R^2=0.654), larger particles (>20µm) form a group of low Th values and small particles (<10µm and <2µm) are located at the opposite end, at high Th values.

3.4 Characterization of sediment fractions

The size fractionation of sediments results in a differentiation of components. Each grain size class is composed of biogenic and lithogenic components with different physical properties (specific surface area and mean grain size), as reported for the samples GeoB1027-2 and PS1769-1 in Table 4. Chemical properties (biogenic opal content and elemental composition) are reported for the samples PS1768-8 and PS1769-1 in Table A1 in appendix

A. The finest particle classes (<20µm) of carbonate sediment contain clay and coccoliths with a mean grain size of 2-6µm and a specific surface area (SSA) of 6-29m²/g. The coarser carbonate fractions (>20µm) mainly consist of foraminifera and their fragments (34-204µm, 4-5m²/g). The finest fractions (<20µm) of the siliceous sediment consist of clay minerals and diatom fragments (3-11µm, 13-57m²/g, 59-80% biogenic opal). All coarser fast sinking particle fractions (>20µm) consist of a mixture of lithogenic particles and radiolarian frustules (Figure 4a, 41-418µm, 2-3m²/g, 3-17% biogenic opal). Diatom shells and their fragments are the main component of the slowly sinking particle fractions (Figure 4b, 30-154µm, 10-11m²/g, 75-82% biogenic opal). Diatoms shells are also present among the fast settling particles.

3.5 Th and U isotopes related to surface area, grain size and elemental composition

To test the relation between the SSA and mean grain size described in 3.4 with the distribution of $^{230}Th_{xs}$ ^{232}Th and $^{238}U_{auth}$ as shown for the fractionated samples GeoB1027-2 and PS1769-1 in Figure 5, Spearman's rho statistic was used to estimate a rank-based measure of association (correlation r and level of significance p). Spearman´s rho is a non-parametric test which is considered to be appropriate for our data as they are small in sample size and do not come from a bivariate normal distribution (Siegel 2001). The specific surface area of the carbonate sample is correlated significantly with $^{230}Th_{xs}$ ($r=0.905$ $p\leq0.01$) and ^{232}Th ($r=0.929$ $p\leq0.01$). $^{238}U_{auth}$ is not correlated ($r=0.381$ $p>0.05$). The SSA of the siliceous sample is correlated with $^{230}Th_{xs}$ ($r=0.943$ $p\leq0.05$), ^{232}Th ($r=0.943$ $p\leq0.05$), and $^{238}U_{auth}$ ($r=1.000$ $p\leq0.01$) only when the fast settling particles are excluded. The best fit of the regression lines is achieved by logarithmic equations. Correlations between mean grain size and the isotopes are apparent but less pronounced. Positive correlations appear between $^{230}Th_{xs}$ and the two alkali metals Rb and Cs. Other elements do not correlate with $^{230}Th_{xs}$ (Figure A1 in appendix A).

4 Discussion

4.1 Grain size distributions

The choice of fractionation techniques affects the grain size fractions. Grain size spectra obtained by pureW-fractionation are finer than by seaW-fractionation, probably because (a) in seawater, the particles are prone to flocculation and not suspended as individual grains, (b) clay that sticks to large particles could be detached during ultrasonication in the pureW-suspension, or (c) suspension in pureW and ultrasonication may partially dissolve or break large particles into fragments.

Both twin core locations show a preferential deposition of fine material at the more rapidly accumulated core, confirming the assumption of particle sorting by lateral sediment transport. The sediments of the Southern Ocean locations are fine-grained (74% in the <10µm class) and probably deposited as aggregates, because particles <10µm behave cohesively (McCave and Hall, 2006). Most of the particulate material is carried vertically downward by aggregates that settle faster than it would be expected for individual particles. Ziervogel and Forster (2005) show that pelagic diatoms potentially increase the rate of particle aggregation, and that diatom bearing aggregates of in vitro experiments (140-200µm) reach 52-104m/d. Mean sinking rates are calculated from sediment trap deployments to be 157m/d in the Southern Ocean (Fischer and Karakas, 2009). Therefore, the "slowly settling particles", as classified in this study, may not have settled as isolated grains through the water column and settling velocities (~26m/d, mean size 154µm) may underestimate velocities found under natural conditions.

The carbonate sediment of the Walvis Ridge locations is less fine grained (28-43% in the <10µm class) than the siliceous twin core sediments. The variations in grain size distributions and carbonate concentrations between the carbonate twin cores can be explained by differences in deposition of fine material or carbonate dissolution. According to Volbers

and Henrich (2002), the carbonate preservation at this depth of Walvis Ridge is good to moderate, but the higher TOC content and the deeper water depth at site GeoB1027 (Table 1) may lead to stronger carbonate dissolution and fragmentation of foraminifera shells than at GeoB1028.

4.2 $^{230}Th_{xs}$ in particle classes

Our hypothesis that particles of the same composition and size from the same water-depth are equilibrated with the same amount of $^{230}Th_{xs}$ adsorbed is confirmed for the finest particles, but not for the coarser particles. This finest fraction (<2µm and <10µm) is the main carrier for $^{230}Th_{xs}$, because it has the largest specific surface area, capturing most ^{230}Th. The specific activity of $^{230}Th_{xs}$ is inversely related to the grain size. Within the siliceous sediment, the adsorption of $^{230}Th_{xs}$ onto the opal-rich fine fractions (<2µm, 61-68% opal) is very strong compared to the opal-rich coarse fractions (>20µm, 75-82% opal). We deduce that the lithogenic (clay mineral) content within the fine fraction is responsible for the strong Th scavenging and that Th has a weak affinity to opal, corroborating the results of Chase et al. (2002), Luo and Ku (1999) and Roy-Barman et al. (2005).

Within coarse fractions (>2µm and >10µm) of the carbonate and siliceous samples, the level of $^{230}Th_{xs}$ adsorption is lower, and the twin cores display some unexpected discrepancies in $^{230}Th_{xs}$ when comparing results of the corresponding size fractions. Even though differences are statistically insignificant (within 2σ-error), we discuss them as they seem to be a systematic feature. Possible explanations for this unexpected result are: (a) The higher $^{230}Th_{xs}$ activities in the rapidly accumulated carbonate sediment may be attributed to the deeper location (453m deeper) thus receiving higher vertical $^{230}Th_{xs}$ fluxes from the water column than the slowly accumulating site. However, after normalizing the $^{230}Th_{xs}$ activities of both twin cores to the same water depth (data not shown here), an unexplained discrepancy between both core sites remains. The difference in water depth (30m) between PS1768 and

PS1769 is negligible for the $^{230}Th_{xs}$ differences. (b) The samples of GeoB1027-2 and GeoB1028-4 differ in their (interpolated) age by 1.7kyr (Table 1). The conditions of sedimentation (water masses, current speed, and sediment supply) may not have been constant during this time period, so that the two samples are potentially not directly comparable concerning their $^{230}Th_{xs}$ activities. In the siliceous twin cores, the age differences should be of minor importance as the samples are from the same (interpolated) age. (c) The differences in Th and U leaching during sieve and settling could potentially be a further reason for the observed $^{230}Th_{xs}$ differences. During the pureW fractionation Th and U leaching from sample PS1768 is 3-4 times stronger than from sample PS1769 (table 2). On the other hand all other fractionations are very similar concerning Th and U leaching, arguing against the leaching scenario.

Summarizing the $^{230}Th_{xs}$ distribution in the grain size classes, we find that the finest material (<2µm) contains 50-90% of the total sediment's $^{230}Th_{xs}$ inventory. This fraction is preferentially deposited at the rapid accumulation sites, and therefore contributes more to the $^{230}Th_{xs}$ inventory than at the slow accumulation sites. Similar results are reported from North Atlantic sediments by Scholten et al. (1994), who find ~90% of $^{230}Th_{xs}$ in the grain size class <6.3µm, and by Thomson et al. (1993) who find 3-fold higher concentrations of $^{230}Th_{xs}$ in the fine fraction (<5µm) than in the coarse fraction (>400µm).

4.3 U in particle classes

Elevated U concentrations can be due to the formation of authigenic U (U_{auth}) under chemically reducing conditions, induced by the high flux of organic carbon. As already reported by Anderson et al. (1998) for several sediment cores in the South Atlantic near 52°S, sediment focusing enhanced the accumulation rates of U_{auth} during Holocene and the LGM. The preferential deposition of small and slowly sinking particles may increase the local flux of organic matter relative to the vertical organic matter flux from surface waters (Anderson et

al., 1998; Beaulieu, 2002; Mollenhauer et al., 2006). Especially unconsolidated organic-rich aggregates at the sediment-water-interface are prone to resuspension at low critical shear velocities (e.g. 0.4-0.8cm/s for diatom derived detritus; Beaulieu, 2003). At both twin core locations, the concentration of total organic matter is more than twice as high at the rapid accumulation site (Table 1), probably enhancing the precipitation of U_{auth}. At the carbonate twin cores, the difference in U_{auth} in bulk samples is relatively small (2.3ppm and 2.1ppm, respectively). The portion of the total U that is authigenic ranges from 84% to 90% (bulk) and from 44% to 90% (grain size fractions, Table A2 in appendix A). In contrast, the twin cores at the siliceous location differ by a factor of ~7 (3.7ppm and 0.5ppm, respectively). The difference of U_{auth} between the twin cores is particularly pronounced in the smallest <2µm fractions (Figure 1 and 2). The portion of the total U that is authigenic at the rapid accumulation site is 90% (bulk) and 26-92% (grain size fractions), and at the slow accumulation site it is 58% (bulk) and 22-89% (grain size fractions). Although the sediment cores are in close proximity, they exhibit contrasting concentrations of U_{auth}, indicating that organic carbon accumulation in this case is the result of sediment redistribution rather than export production.

4.4 Th and U related to the specific surface area

The observed distribution of $^{230}Th_{xs}$ corroborate the general hypothesis that ^{230}Th adsorption onto particles depends on grain size and specific surface area (SSA, Figure 5). Surprisingly, however, the fast sinking particles do not fit on the logarithmic regression line, revealing a relatively high $^{230}Th_{xs}$ concentration relative to their surface area. This could be due to differences in elemental composition (see Table A1 and Figure A1 in appendix A), which may enhance or reduce the particle's affinity for ^{230}Th adsorption**.**

The correlation of ^{232}Th with the SSA (Figure 5) can be attributed to lithogenic (clay mineral) particles rich in ^{232}Th, which generally reside in smaller particle size classes with

higher SSA. This would indicate the preferential affinity of $^{230}Th_{xs}$ to lithogenic material, which is further supported by the linear correlation between $^{230}Th_{xs}$ and ^{232}Th (Figure 3).

4.5 Focusing factor and $^{230}Th_{xs}$ normalization corrected for particle sorting

The bulk focusing factor is calculated for PS1768 (12-24kyr) and PS1769 (16-24kyr) to be Ψ=5.9 and 3.2, respectively. This means that mass accumulation is largely controlled by lateral sediment flux, and it is twice faster at PS1768 than at PS1769. In the following section, we calculate to which extent particle sorting could potentially bias the focusing factor and $^{230}Th_{xs}$ normalized fluxes of the studied samples. The conventional focusing factor (Ψ) is calculated for a core section between two dated core depths and based on the $^{230}Th_{xs}$ inventory averaged over this core depth (François et al. 2004). In the present study, the focusing factor that is corrected for the particle sorting effect (Ψ_c) is derived from only one single sample depth, representing the whole core section, as no further size-fractionated $^{230}Th_{xs}$ data is available.

Our assumption for particle sorting correction is that the lateral sediment flux is controlled by preferential transport of fine material. The vertical particle flux consequently must have been coarser in grain size distribution than measured in the bulk sample. As grain size distributions of the vertical and lateral fluxes are unknown, we need to postulate a certain grain size distribution with predefined portions of fine and coarse particles within one of the fluxes. From this we are able to calculate the grain size weighted $^{230}Th_{xs}$ within the lateral (or vertical) sediment flux. Appendix B shows how the fluxes can be calculated for any choice of grain size distribution in the lateral (vertical) flux. If we make the simplifying assumption that the lateral flux consists only of small particles, the problem reduces to the situation that the excess Th sedimentation is exclusively supplied by small advected particles, which can be expressed with equation 1

$$x = \frac{T_m}{T_k}\left(1 - \frac{1}{\Psi}\right) \quad (1)$$

where x is the portion of the lateral sediment flux related to the sedimentation rate, Ψ is the focusing factor measured, T_m is the bulk $^{230}Th_{xs}$ activity (dpm/g) in the sediment, T_k is the $^{230}Th_{xs}$ activity (dpm/g) in the small particle fraction. With x we are able to calculate the grain size corrected Ψ_c:

$$\Psi_c = \frac{1}{1-x} = \frac{1}{1 - \frac{T_m}{T_k}\left(1 - \frac{1}{\Psi}\right)} \quad (2)$$

According to the corrected focusing factor Ψ_c the preserved vertical mass flux F_V [g/cm²/kyr] needs to be corrected (F_{Vc}):

$$F_{Vc} = F_V \frac{\Psi}{\Psi_c} \quad (3)$$

As an alternative, for the calculation of x the vertical $^{230}Th_{xs}$ flux can be assumed to be carried by the large particles and a fraction of the small ones calculated to match the water column derived ^{230}Th production. In this case the lateral sediment flux consists of only small particles which transport the difference between the total accumulated $^{230}Th_{xs}$ and the water column derived $^{230}Th_{xs}$. This is a special case of the derivation given in appendix B and yields the same solution.

The calculations are performed with grain size and $^{230}Th_{xs}$ data sets of both methods (pureW and seaW) and results are equivalent within a range of 0.1-5.5%. In most cases the data from pureW-fractionated samples produce a stronger bias than the seaW-fractionations. The following discussion refers only to data from the seaW method (Table 5), which is expected to better match natural conditions. With the simplifying assumption that the lateral flux consists of only “small particles” we calculate three scenarios of Ψ_c with “small particles” defined as (a) <125µm, (b) <63µm, and (c) <10µm. For example, if the lateral flux

at core site PS1768-8 (Ψ=5.9) is assumed to be limited to particles <125µm, *x* equals 0.82, i.e. a mixing ratio of 82% lateral flux with 18% vertical flux is required, resulting in Ψ_c=5.5. If the lateral flux is assumed to be limited to particles <63µm the calculation would yield *x*=0.8 and Ψ_c=5.0. A scenario of lateral flux of particles <10µm (*x*=0.69) results in Ψ_c=3.2. This means that the actual degree of focusing is overestimated accordingly due to particle sorting effects. As a consequence higher vertical mass flux rates than estimated using the classical bulk ^{230}Th correction method are required in order to balance lateral fluxes composed primarily of smaller grains. This effect becomes stronger with smaller predominant grain size of laterally supplied material. In case of particles <10µm at PS1768 and PS1769, the vertical fluxes F_V would increase with respect to those estimated using the bulk $^{230}Th_{xs}$ method from 1.7 to 3.1g/cm²/kyr and from 1.4 to 2.1g/cm²/kyr, respectively (Table 5).

It is likely that sand-sized particles >63µm quickly fall out of suspension (McCave and Gross, 1991), while fine material <63µm is transported over longer distances. A current driven sorting of particles smaller than 2µm is unlikely, because particles <7-11µm behave cohesively, are transported as flocs, and are not subject to sorting effects (McCave et al., 1995). A selective deposition of only fines <10µm should be considered as a maximum sorting effect that is likely to occur only under regimes dominated by weak bottom currents. Strong bottom current regimes as prevailing in the Antarctic circumpolar current region are more likely to transport also coarser particles. Therefore we consider selective deposition of particle classes <63µm as the more likely scenarios for the locations of this study.

Isotopes of Th and U are not equally distributed within particle classes and therefore the sorting effect bears the potential to induce a decoupling of Th and U isotopic records. However, in the scenarios $\Psi_{<10\mu m}$ and $\Psi_{<63\mu m}$, the isotopic decoupling is negligible or not evident: e.g. in the case of PS1768, the lateral flux accounts for 83% of total deposited ^{230}Th, 81-83% of total deposited ^{238}U, and 83-88% of total deposited ^{232}Th.

5 Conclusions

5.1 Technique of sediment fractionation

The comparison of two fractionation methods reveals that the choice of sample pretreatment and fractionation fluid affects the distributions of grain sizes, Th and U. Generally, the seaW-technique has the disadvantages that (a) small grain sizes cannot be separated properly due to the flocculation effect and (b) that complex interactions between the natural seawater matrix (e.g. with high U content) and the suspended particles lead to experimental conditions that are difficult to reproduce. The pureW-technique turns out to be more reproducible, but it potentially affects the particles by dissolution and/or comminution. As a consequence for future experiments, we suggest to use a gentle fractionation method with artificial seawater (free of Th and U) and to monitor Th and U in the supernatant, because leaching and/or uptake of Th and U during fractionation could introduce an error in calculating grain size fractionated $^{230}Th_{xs}$.

5.2 $^{230}Th_{xs}$ in different grain-size and lithologic classes

The main carrier for the sedimentary $^{230}Th_{xs}$-signal is the fine sediment fraction, whereas coarse particles carry a much lower $^{230}Th_{xs}$ activity. This general distribution pattern is observed at all locations. However, in the siliceous sediment, the affinity of $^{230}Th_{xs}$ to fine and lithogenic-rich material is more pronounced than in the carbonate sediment. The coarse carbonate fractions (mainly foraminifera) carry a relatively large $^{230}Th_{xs}$ signal. In contrast, the biogenic opal content does not significantly affect the $^{230}Th_{xs}$ concentrations. Some coarse particle fractions reveal differences between the twin cores, which cannot be readily explained. The identical $^{230}Th_{xs}$ specific activities within the finest sediment fractions of the twin cores suggests that redistributed sediment particles must have the same source, and that the distance of redistribution cannot have been very large, supporting the $^{230}Th_{xs}$-based

approach to correct for sediment redistribution. The fine material is preferentially deposited at the rapidly accumulated locations potentially influencing the $^{230}Th_{xs}$ inventory.

5.3 Implications for $^{230}Th_{xs}$ as constant flux tracer

Our study clearly illustrates that particle sorting during lateral transport has an effect on $^{230}Th_{xs}$ inventories of bulk sediments. A systematically higher $^{230}Th_{xs}$ concentration is found in the fine grain size fractions. As a result, $^{230}Th_{xs}$ inventories of focused sediments are biased towards the contribution of fine-grained sediments, which results generally in overestimating the effect of focusing and underestimating the actual vertical particle fluxes in focused sediments. In general, we can state that the smaller the particles and the higher the clay mineral content within the laterally transported sediment with respect to the vertical component, the stronger is the grain size bias on the focusing factor. Strongest grain size bias would accordingly occur in those regimes dominated by weak bottom currents, where the finest grain size fractions are preferentially deposited. At locations of very high focusing factors as e.g. in the equatorial Pacific, we suppose against the background of our data, that $^{230}Th_{xs}$ accumulation in sediments is controlled by processes of sedimentology (i.e. winnowing/focusing, cf. Kienast et al., 2007, Kusch et al., 2010, Loubere et al., 2004, Marcantonio et al., 2001, Siddall et al., 2008) rather than by an increased scavenging efficiency (cf. Broecker, 2008, Lyle et al., 2005, Thomas et al., 2000). Consequently we expect high focusing factors to be lower and the vertical sediment fluxes to be higher after applying a grain size correction.

As illustrated for the core PS1768-8, the $^{230}Th_{xs}$ normalized vertical flux rate is higher after grain size correction (F_{Vc}=3.1g/cm²/kyr at maximum). However, the error introduced by using $^{230}Th_{xs}$ normalization is low compared to a sediment flux rate that has not been $^{230}Th_{xs}$ normalized (MAR=10.1g/cm²/kyr). Thus, the normalization procedure is still a considerable improvement compared to the uncorrected fluxes. This leads us to conclude that $^{230}Th_{xs}$

normalization is still the method of choice to unravel strong lateral sediment dislocation events.

Acknowledgements

Ingrid Stimac is thanked for technical support in the radioisotope laboratory. We are grateful to Ute Bock for explaining the utilization of the scanning electron microscope, to Rita Fröhlking for assistance in determining biogenic opal, and to Jan-Berend Stuut and Inka Meyer for their help with laser particle size analysis. We thank Gerhard Kuhn who generously provided sedimentology data and Rainer Gersonde for providing sediment samples. Siliceous sediments (cores PS1768-8 and PS1769-1) and carbonate sediments (cores GeoB1027-2 and GeoB1028-4) were recovered during expeditions with Polarstern (ANT-VIII/3) and Meteor (M6/6), respectively. The funding for this work was provided by a Helmholtz Young Investigators Group grant to GM. We thank Martin Frank and three anonymous reviewers for their useful comments which helped improving the manuscript.

References

Ackermann, F., Bergmann, H., Schleichert, U., 1983. Monitoring of heavy metals in coastal and estuarine sediments - a question of grain-size: <20µm versus >60µm. Environmental Technology 4, 317 - 328.

Anderson, R.F., Kumar, N., Mortlock, R.A., Froelich, P.N., Kubik, P., Dittrich-Hannen, B., Suter, M., 1998. Late-Quaternary changes in productivity of the Southern Ocean. Journal of Marine Systems 17, 497-514.

Bacon, M.P., Anderson, R.F., 1982. Distribution of Thorium Isotopes between Dissolved and Particulate Forms in the Deep-Sea. Journal of Geophysical Research - Oceans and Atmospheres 87, 2045-2056.

Bacon, M.P., 1984. Glacial to Interglacial Changes in Carbonate and Clay Sedimentation in the Atlantic-Ocean Estimated from Th-230 Measurements. Isotope Geoscience 2, 97-111.

Barbanti, A., Bothner, M.H., 1993. A procedure for partitioning bulk sediments into distinct grain-size fractions for geochemical analysis. Environmental Geology 21, 3-13.

Beaulieu, S.E., 2002. Accumulation and fate of phytodetritus on the sea floor, in: Oceanography and Marine Biology, Vol 40. Taylor & Francis Ltd, London, 171-232.

Beaulieu, S.E., 2003. Resuspension of phytodetritus from the sea floor: A laboratory flume study. Limnology and Oceanography 48, 1235-1244.

Bianchi, G.G., McCave, I.N., 2000. Hydrography and sedimentation under the deep western boundary current on Björn and Gardar Drifts, Iceland Basin. Marine Geology 165, 137-169.

Broecker, W., 2008. Excess sediment ^{230}Th: Transport along the sea floor or enhanced water column scavenging? Global Biogeochemical Cycles 22, 1-4.

Brunauer, S., Emmett, P.H., Teller, E., 1938. Adsorption of Gases in Multimolecular Layers. Journal of the American Chemical Society 60, 309-319.

Chase, Z., Anderson, R.F., Fleisher, M.Q., Kubik, P.W., 2002. The influence of particle composition and particle flux on scavenging of Th, Pa and Be in the ocean. Earth and Planetary Science Letters 204, 215-229.

Dezileau, L., Bareille, G., Reyss, J.L., Lemoine, F., 2000. Evidence for strong sediment redistribution by bottom currents along the southeast Indian ridge. Deep Sea Research Part I: Oceanographic Research Papers 47, 1899-1936.

Diekmann, B., Fütterer, D., Grobe, H., Hillenbrand, C.-D., Kuhn, G., Michels, K., Petschick, R., Pirrung, M., 2003. Terrigenous sediment supply in the polar to temperate South Atlantic: Land-ocean links of environmental changes during the late quarternary, in: Wefer, G., Mulitza, S., Ratmeyer, V. (Eds), The South Atlantic in the Late Quarternary. Reconstructions of Material Budgets and Current Systems. Springer, Berlin, 375-399.

Fischer, G., Karakas, G., 2009. Sinking rates and ballast composition of particles in the Atlantic Ocean: implications for the organic carbon fluxes to the deep ocean. Biogeosciences 6, 85-102.

Förstner, U., 2004. Traceability of sediment analysis. TrAC Trends in Analytical Chemistry 23, 217-236.

François, R., Bacon, M.P., Suman, D.O., 1990. Thorium-230 Profiling in Deep-Sea Sediments: High-Resolution Records of Flux and Dissolution of Carbonate in the Equatorial Atlantic During the Last 24,000 Years. Paleoceanography 5, 761-787

François, R., Bacon, M.P., Altabet, M.A., Labeyrie, L.D., 1993. Glacial/Interglacial Changes in Sediment Rain Rate in the SW Indian Sector of Subantarctic Waters as Recorded by ^{230}Th, ^{231}Pa, U, and delta^{15}N. Paleoceanography 8, 611-629.

François, R., Frank, M., Rutgers van der Loeff, M.M., Bacon, M.P., 2004. ^{230}Th normalization: An essential tool for interpreting sedimentary fluxes during the late Quaternary Paleoceanography 19, PA1018, doi:10.1029/2003PA000939.

François, R., Frank, M., Rutgers van der Loeff, M., Bacon, M.P., Geibert, W., Kienast, S., Anderson, R.F., Bradtmiller, L., Chase, Z., Henderson, G., Marcantonio, F., Allen, S.E., 2007. Comment on "Do geochemical estimates of sediment focusing pass the sediment test in the equatorial Pacific?" by M. Lyle et al. Paleoceanography 22, PA1216, doi:10.1029/2005PA001235.

Frank, M., Mangini, A., Gersonde, R., Rutgers van der Loeff, M., Kuhn, G., 1996. Late Quaternary sediment dating and quantification of lateral sediment redistribution applying $^{230}Th_{ex}$: a study from the eastern Atlantic sector of the Southern Ocean. Geologische Rundschau 85, 554-566.

Frank, M., Gersonde, R., Mangini, A., 1999. Sediment Redistribution, $^{230}Th_{ex}$-Normalization and Implications for the Reconstruction of Particle Flux and Export Paleoproductivity, in: G., F., Wefer, G. (Eds), Use of Proxies in Paleoceanography: Examples from the South Atlantic. Springer, Berlin Heidelberg, 409-426.

Frank, M., Gersonde, R., Rutgers van der Loeff, M., Bohrmann, G., Nürnberg, C.C., Kubik, P., Suter, M., Mangini, A., 2000. Similar glacial and interglacial export bioproductivity in the Atlantic sector of the Southern Ocean: Multiproxy evidence and implications for glacial atmospheric CO_2. Paleoceanography 15, 642-658.

Geibert, W., Usbeck, R., 2004. Adsorption of thorium and protactinium onto different particle types: experimental findings. Geochimica et Cosmochimica Acta 68, 1489-1501.

Gersonde, R., Hempel, G., 1990. Die Expedition ANTARKTIS-VIII/3 und VIII/4 mit FS "Polarstern" 1989. Berichte zur Polarforschung 74.

Guo, L.D., Chen, M., Gueguen, C., 2002. Control of Pa/Th ratio by particulate chemical composition in the ocean. Geophys. Res. Lett. 29, 1961, doi:10.1029/2002GL015666.

Hansen, R.G., Ring, E.J., 1983. The Preparation and Certification of a Uranium reference material, Council for Mineral Technology, Randburg, South Africa.

Henderson, G.M., Heinze, C., Anderson, R.F., Winguth, A.M.E., 1999. Global distribution of the ^{230}Th flux to ocean sediments constrained by GCM modelling. Deep Sea Research Part I: Oceanographic Research Papers 46, 1861-1893.

Henderson, G.M., Anderson, R.F., 2003. The U-series toolbox for paleoceanography, in: Uranium-Series Geochemistry. Mineralogical Soc America, Washington, 493-531.

Horwitz, E.P., Chiarizia, R., Dietz, M.L., Diamond, H., Nelson, D.M., 1993. Separation and preconcentration of actinides from acidic media by extraction chromatography. Analytica Chimica Acta 281, 361-372.

Kienast, S.S., Kienast, M., Mix, A.C., Calvert, S.E., François, R., 2007. Thorium-230 normalized particle flux and sediment focusing in the Panama Basin region during the last 30,000 years. Paleoceanography 22,

Klein, C., Dana, J.D., Hurlbut, C.S., 1985. Manual of mineralogy (after James D. Dana), Chapter 11 Systematic Mineralogy Part IV: Silicates. pp.366-467. Wiley, New York.

Koopmann, C., Prange, A., 1991. Multielement determination in sediments from the German Wadden Sea--investigations on sample preparation techniques. Spectrochimica Acta Part B: Atomic Spectroscopy 46, 1395-1402.

Köster, E., 1964. Granulometrische und morphometrische Meßmethoden an Mineralkörnern, Steinen und sonstigen Stoffen, Ferdinand Enke Verlag, Stuttgart.

Kusch, S., Eglinton, T.I., Mix, A.C., Mollenhauer, G., 2010. Timescales of lateral sediment transport in the Panama Basin as revealed by radiocarbon ages of alkenones, total organic carbon and foraminifera. Earth and Planetary Science Letters 290, 340-350.

Loubere, P., Mekik, F., François, R., Pichat, S., 2004. Export fluxes of calcite in the eastern equatorial Pacific from the Last Glacial Maximum to present Paleoceanography 19, doi:10.1029/2003PA000986.

Luo, S., Ku, T.-L., 1999. Oceanic $^{231}Pa/^{230}Th$ ratio influenced by particle composition and remineralization. Earth and Planetary Science Letters 167, 183-195.

Lyle, M., Mitchell, N., Pisias, N., Mix, A., Martinez, J.I., Paytan, A., 2005. Do geochemical estimates of sediment focusing pass the sediment test in the equatorial Pacific? Paleoceanography 20, PA1005, doi:10.1029/2004PA001019.

Lyle, M., Pisias, N., Paytan, A., Martinez, J.I., Mix, A., 2007. Reply to comment by R. Francois et al. on "Do geochemical estimates of sediment focusing pass the sediment test in the equatorial Pacific?": Further explorations of 230Th normalization. Paleoceanography 22, PA1217, doi:10.1029/2006PA001373.

Marcantonio, F., Anderson, R.F., Higgins, S.M., Stute, M., Schlosser, P., Kubik, P., 2001. Sediment focusing in the central equatorial Pacific ocean Paleoceanography 16, 260-267.

Martínez-Garcia, A., Rosell-Melé, A., Geibert, W., Gersonde, R., Masqué, P., Gaspari, V., Barbante, C., 2009. Links between iron supply, marine productivity, sea surface temperature, and CO_2 over the last 1.1 Ma. Paleoceanography 24, PA1207, doi:10.1029/2008PA001657.

McCave, I.N., Gross, T.F., 1991. In-situ measurements of particle settling velocity in the deep sea. Marine Geology 99, 403-411.

McCave, I.N., Manighetti, B., Robinson, S.G., 1995. Sortable Silt and Fine Sediment Size/Composition Slicing: Parameters for Palaeocurrent Speed and Palaeoceanography. Paleoceanography 10, 593-610.

McCave, I.N., Hall, I.R., 2006. Size sorting in marine muds: Processes, pitfalls, and prospects for paleoflow-speed proxies. Geochem. Geophys. Geosyst. 7, Q10N05, doi:10.1029/2006GC001284

Mollenhauer, G., McManus, J.F., Benthien, A., Muller, P.J., Eglinton, T.I., 2006. Rapid lateral particle transport in the Argentine Basin: Molecular ^{14}C and $^{230}Th_{xs}$ evidence Deep Sea Research Part I: Oceanographic Research Papers 53, 1224-1243.

Moore, R.M., Hunter, K.A., 1985. Thorium adsorption in the ocean: reversibility and distribution amongst particle sizes. Geochimica et Cosmochimica Acta 49, 2253-2257.

Müller, 2003a. Bulk elemental composition of sediment core GeoB1028-4. http://www.pangaea.de/. doi:10.1594/PANGAEA.132799

Müller, 2003b. Carbonate and carbon content of sediment core GeoB1027-2. http://www.pangaea.de/. doi:10.1594/PANGAEA.96367

Müller, P. J., and R. Schneider (1993). An automated leaching method for the determination of opal in sediments and particulate matter. Deep Sea Research Part I: Oceanographic Research Papers, 40, 425-444.

Nozaki, Y., Horibe, Y., Tsubota, H., 1981. The water column distributions of thorium isotopes in the western North Pacific. Earth and Planetary Science Letters 54, 203-216.

Nürnberg, C.C., Bohrmann, G., Schlüter, M., Frank, M., 1997. Barium Accumulation in the Atlantic Sector of the Southern Ocean: Results from 190,000-Year Records. Paleoceanography 12, 594-603.

Ohkouchi, N., Eglinton, T.I., Keigwin, L.D., Hayes, J.M., 2002. Spatial and Temporal Offsets Between Proxy Records in a Sediment Drift. Science 298, 1224-1227.

Robinson, L.F., Noble, T.L., McManus, J.F., 2008. Measurement of adsorbed and total $^{232}Th/^{230}Th$ ratios from marine sediments. Chemical Geology 252, 169-179.

Roy-Barman, M., Jeandel, C., Souhaut, M., Rutgers van der Loeff, M., Voege, I., Leblond, N., Freydier, R., 2005. The influence of particle composition on thorium scavenging in the NE Atlantic Ocean (POMME experiment). Earth and Planetary Science Letters 240, 681-693.

Roy-Barman, M., Lemaître, C., Ayrault, S., Jeandel, C., Souhaut, M., Miquel, J.C., 2009. The influence of particle composition on Thorium scavenging in the Mediterranean Sea. Earth and Planetary Science Letters 286, 526-534.

Rutgers van der Loeff, M.M., Moore, W.S., 1999. Determination of natural radioactive tracers, in: Grasshoff, K., Kremling, K., Ehrhardt, M. (Eds), Methods of Seawater Analysis. Wiley-VCH, Weinheim, 365-397.

Rutgers van der Loeff, M.M., Meyer, R., Rudels, B., Rachor, E., 2002. Resuspension and particle transport in the benthic nepheloid layer in and near Fram Strait in relation to faunal abundances and ^{234}Th depletion. Deep Sea Research Part I: Oceanographic Research Papers 49, 1941-1958.

Rutgers van der Loeff, M.M., Geibert, W., 2008. Chapter 7 U- and Th-Series Nuclides as Tracers of Particle Dynamics, Scavenging and Biogeochemical Cycles in the Oceans, in: Krishnaswami, S., Cochran, K.J. (Eds), U-Th Series Nuclides in Aquatic Systems. Elsevier, 227-268.

Santschi, P.H., Murray, J.W., Baskaran, M., Benitez-Nelson, C.R., Guo, L.D., Hung, C.C., Lamborg, C., Moran, S.B., Passow, U., Roy-Barman, M., 2006. Thorium speciation in seawater. Marine Chemistry 100, 250-268.

Scholten, J.C., Botz, R., Paetsch, H., Stoffers, P., 1994. $^{230}Th_{ex}$ flux into Norwegian-Greenland Sea sediments: Evidence for lateral sediment transport during the past 300,000 years. Earth and Planetary Science Letters 121, 111-124.

Siddall, M., Anderson, R.F., Winckler, G., Henderson, G.M., Bradtmiller, L.I., McGee, D., Franzese, A., Stocker, T.F., Müller, S.A., 2008. Modeling the particle flux effect on distribution of ^{230}Th in the equatorial Pacific. Paleoceanography 23, PA2208, doi:10.1029/2007PA001556.

Siddall, M., Henderson, G.M., Edwards, N.R., Frank, M., Müller, S.A., Stocker, T.F., Joos, F., 2005. ^{231}Pa/^{230}Th fractionation by ocean transport, biogenic particle flux and particle type. Earth and Planetary Science Letters 237, 135-155.

Siegel, S., 2001. Nichtparametrische Statistische Methoden. 5. unveränd. Aufl. Eschborn bei Frankfurt a.M., Verlag Dietmar Klotz GmbH.

Suman, D.O., Bacon, M.P., 1989. Variations in Holocene sedimentation in the North American Basin determined from ^{230}Th measurements. Deep Sea Research Part A. Oceanographic Research Papers 36, 869-878.

Syvitski, J.P.M., Asprey, K.W., Clattenburg, D.A., 1991. Principles, design, and calibration of settling tubes, in: Syvitski, J.P.M. (Ed) Principles, methods, and application of paricle size analysis. Cambridge University Press, Cambridge, 45-63.

Thomas, E., Turekian, K.K., Wei, K.Y., 2000. Productivity Control of Fine Particle Transport to Equatorial Pacific Sediment. Global Biogeochemical Cycles 14, 945-955.

Thomson, J., Colley, S., Anderson, R., Cook, G.T., MacKenzie, A.B., Harkness, D.D., 1993. Holocene Sediment Fluxes in the Northeast Atlantic from $^{230}Th_{excess}$ and Radiocarbon Measurements. Paleoceanography 8, 631-650.

Van Ierland, E.T. and Peperzak, L., 1984. Separation of marine seston and density determination of marine diatoms by density gradient centrifugation. Journal of Plankton Research 6, 29-44.

Volbers, A.N.A., Henrich, R., 2002. Present water mass calcium carbonate corrosiveness in the eastern South Atlantic inferred from ultrastructural breakdown of Globigerina bulloides in surface sediments. Marine Geology 186, 471-486.

Zielinski, U., Gersonde, R., Sieger, R., Fütterer, D., 1998. Quaternary Surface Water Temperature Estimations: Calibration of a Diatom Transfer Function for the Southern Ocean. Paleoceanography 13, 385-388.

Ziervogel, K., Forster, S., 2005. Aggregation and sinking behaviour of resuspended fluffy layer material. Continental Shelf Research 25, 1853-1863.

Figure captions

Figure 1: Distribution of Th and U isotopes by grain size classes of the carbonate sediment at sites of rapid accumulation (GeoB1027-2, white bars) and slow accumulation (GeoB1028-4, grey bars). The results of two fractionation techniques are shown (purified water with ultrasonication and natural seawater without ultrasonication, error bars are ±2σ).

Figure 2: Distribution of Th and U isotopes by grain size classes of the siliceous sediment at sites of rapid accumulation (PS1768-8, white bars) and slow accumulation (PS1769-1, grey bars). The grain size classes 20-63µm, 63-125µm, and >125µm are separated into slowly settling (opal-rich) and fast settling (lithogenic-rich) particle classes. The results of two fractionation techniques are shown (purified water with ultrasonication and natural seawater without ultrasonication, error bars are ±2σ).

Figure 3: Scatter plot of $^{230}Th_{xs}$ and ^{232}Th activities in all analyzed grain size fractions of siliceous and carbonate samples.

Figure 4a and 4b: SEM photographs of the largest grain size fraction (>125µm) of PS1769-1. This sediment sample was separated into (a) a fast settling particle class containing rock fragments and radiolarians and (b) a slowly settling particle class containing mainly diatoms.

Figure 5: Scatter plot of the specific surface area (SSA) and the mean grain size with $^{230}Th_{xs}$ ^{232}Th and $^{238}U_{auth}$ for the size fractions (seawater fractionation) of the samples GeoB1027-2 and PS1769-1. The isotopes show inverse correlations with mean grain

sizes and positive correlations with SSA. A logarithmic function fits best to the SSA – Th/U correlation.

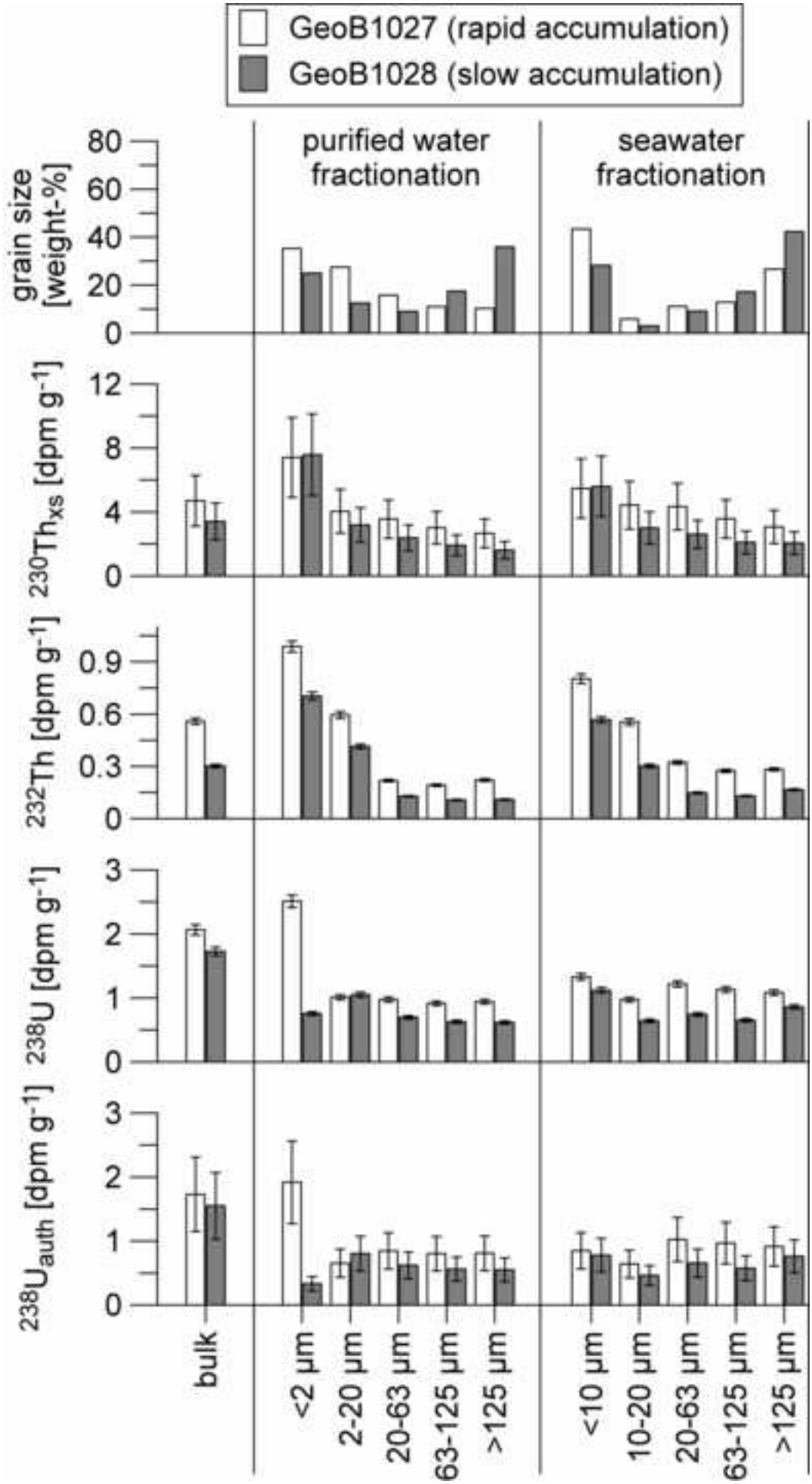
GeoB1027 (rapid accumulation)
GeoB1028 (slow accumulation)
purified water fractionation
seawater fractionation
grain size [weight-%]
$^{230}Th_{xs}$ [dpm g^{-1}]
^{232}Th [dpm g^{-1}]
^{238}U [dpm g^{-1}]
$^{238}U_{auth}$ [dpm g^{-1}]
bulk
<2 µm
2-20 µm
20-63 µm
63-125 µm
>125 µm
<10 µm
10-20 µm
20-63 µm
63-125 µm
>125 µm

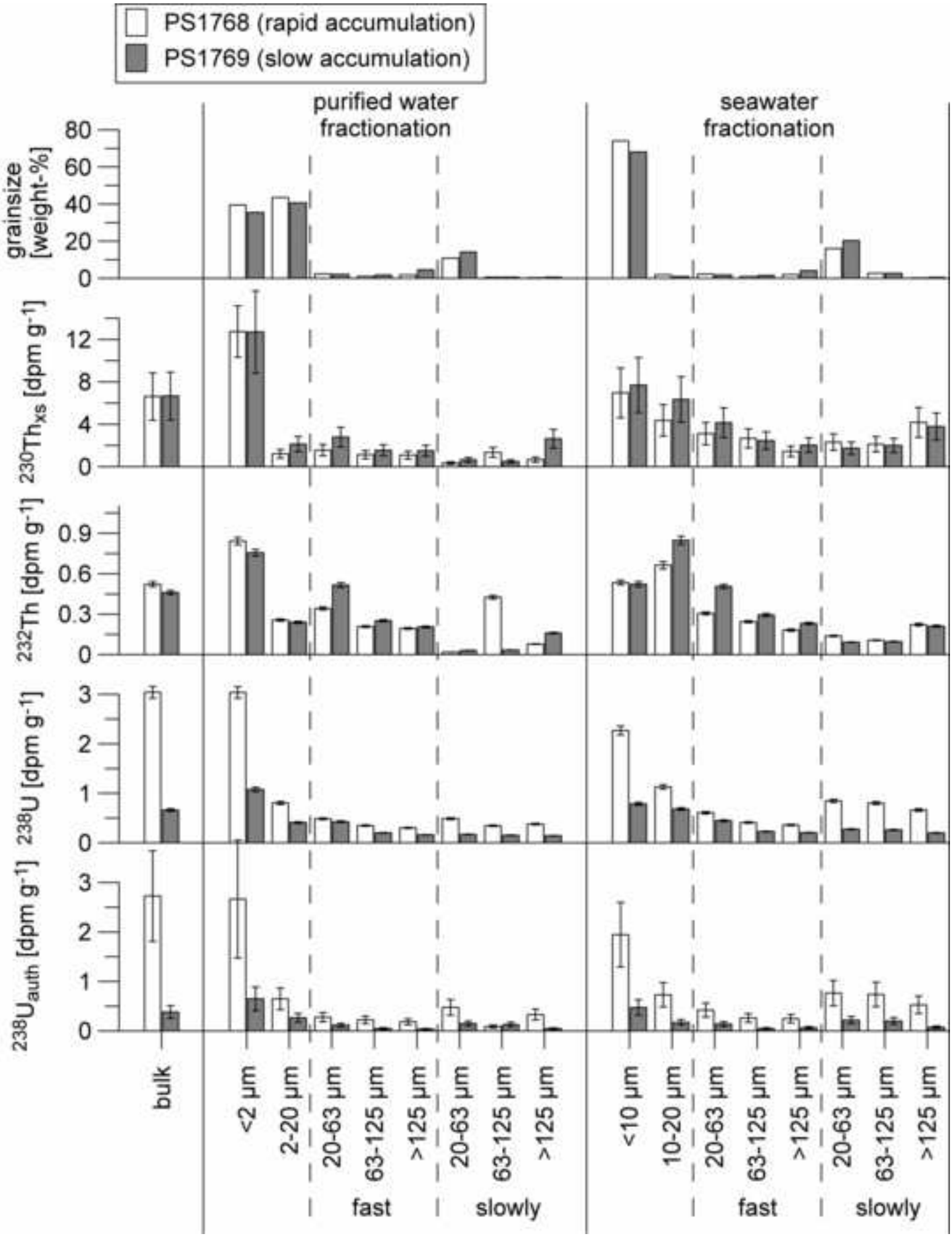
PS1768 (rapid accumulation)
PS1769 (slow accumulation)
purified water fractionation
seawater fractionation
grainsize [weight-%]
$^{230}Th_{xs}$ [dpm g^{-1}]
^{232}Th [dpm g^{-1}]
^{238}U [dpm g^{-1}]
$^{238}U_{auth}$ [dpm g^{-1}]
bulk
<2 µm
2-20 µm
20-63 µm
63-125 µm
>125 µm
20-63 µm
63-125 µm
>125 µm
<10 µm
10-20 µm
20-63 µm
63-125 µm
>125 µm
20-63 µm
63-125 µm
>125 µm
fast
slowly
fast
slowly

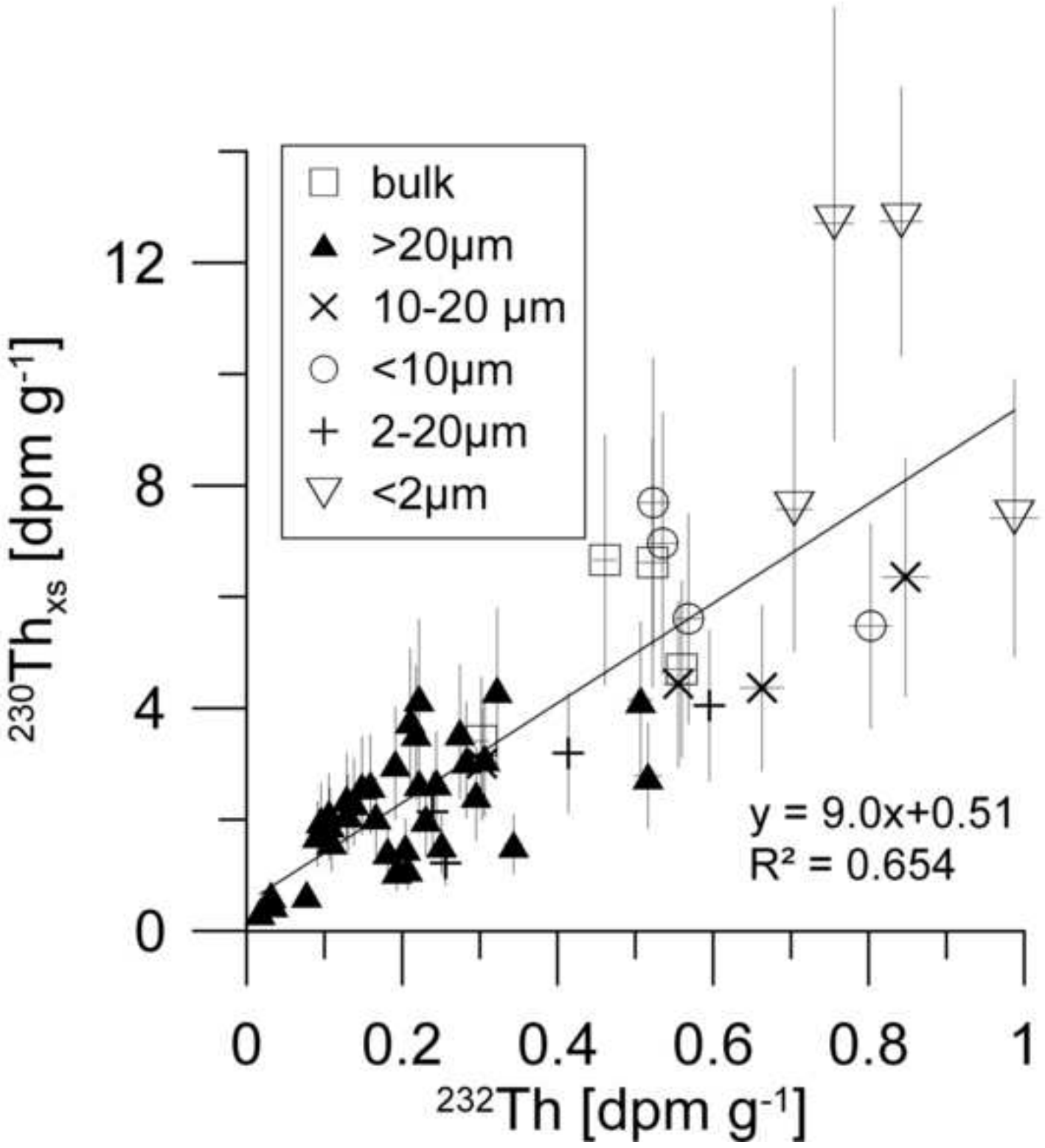
bulk
>20µm
10-20 µm
<10µm
2-20µm
<2µm
y = 9.0x+0.51
R² = 0.654
230Thxs [dpm g-1]
232Th [dpm g-1]
0
4
8
12
0
0.2
0.4
0.6
0.8
1

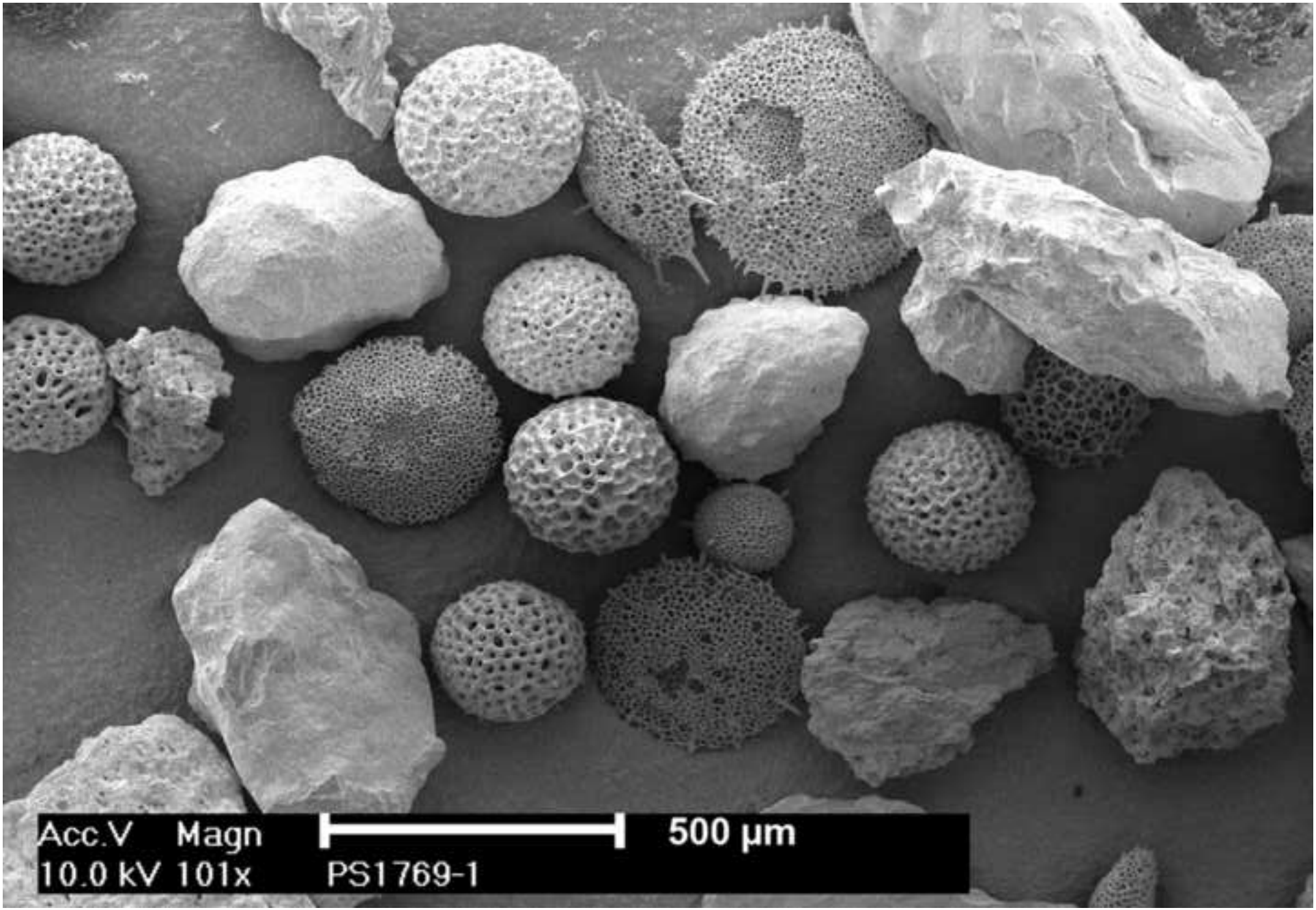
Acc.V Magn
10.0 kV 101x
PS1769-1
500 µm

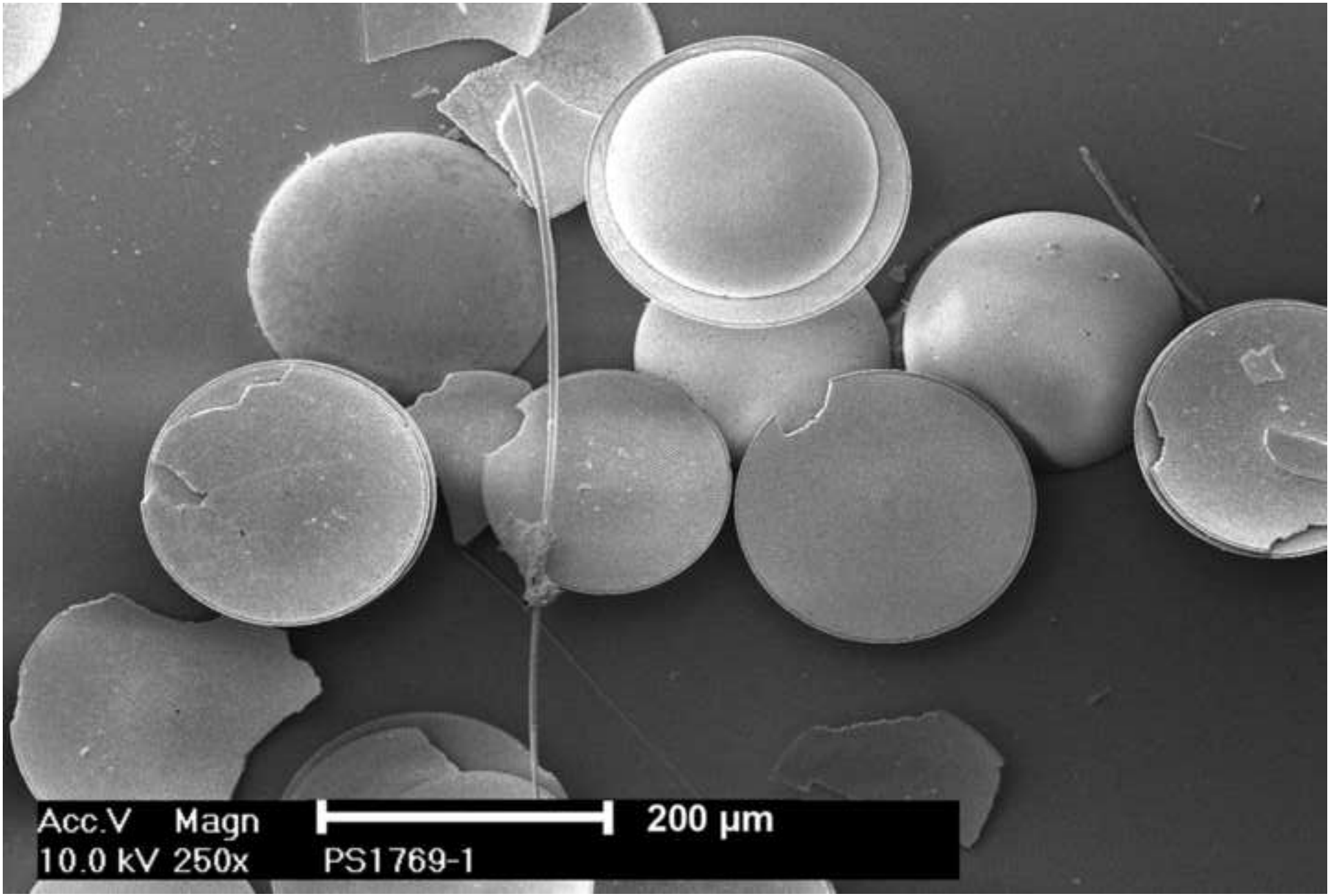
Acc.V Magn
10.0 kV 250x
PS1769-1
200 µm

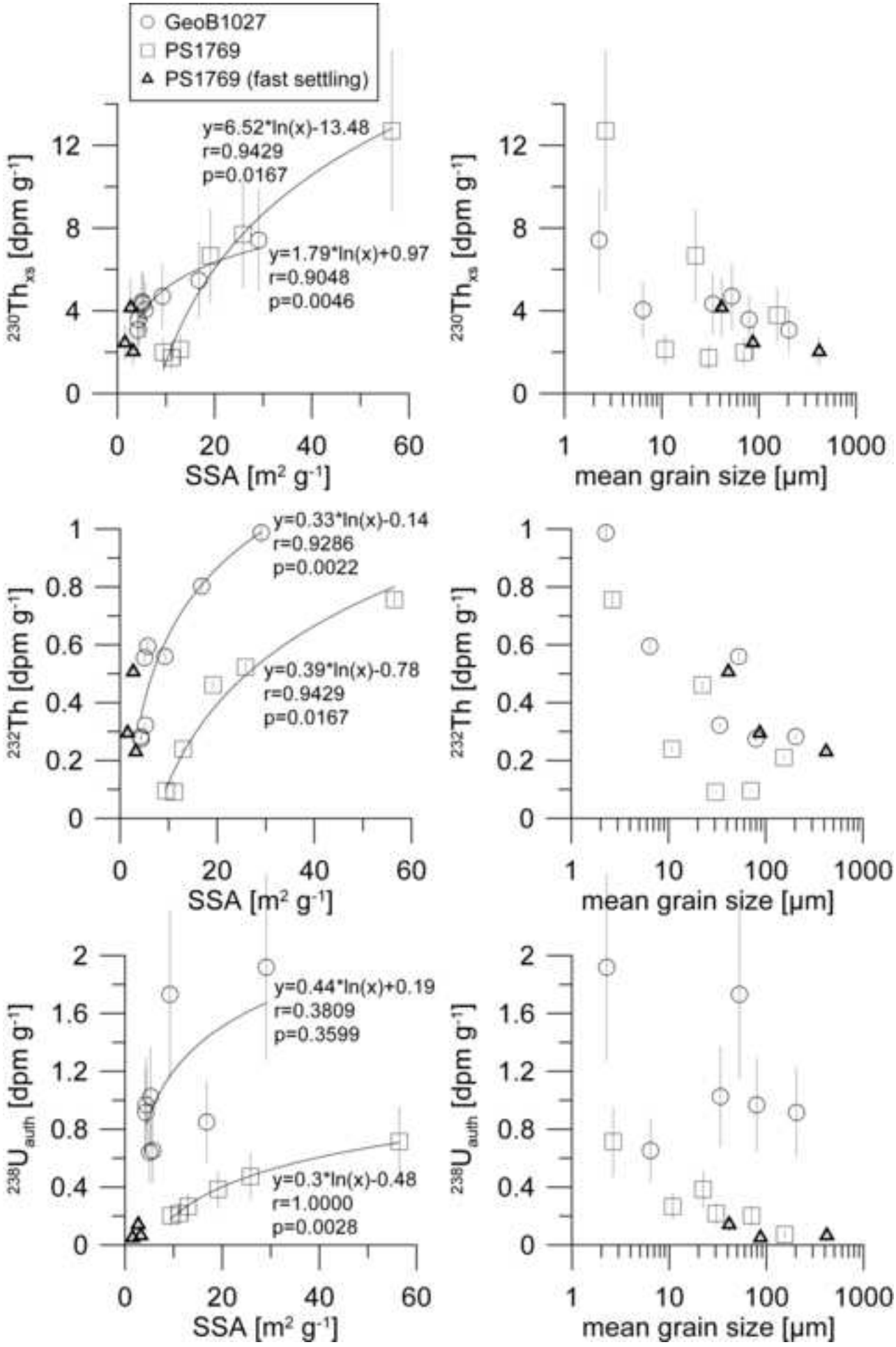
GeoB1027
PS1769
PS1769 (fast settling)
y=6.52*ln(x)-13.48
r=0.9429
p=0.0167
y=1.79*ln(x)+0.97
r=0.9048
p=0.0046
230Thxs [dpm g-1]
SSA [m2 g-1]
mean grain size [µm]
y=0.33*ln(x)-0.14
r=0.9286
p=0.0022
y=0.39*ln(x)-0.78
r=0.9429
p=0.0167
232Th [dpm g-1]
y=0.44*ln(x)+0.19
r=0.3809
p=0.3599
y=0.3*ln(x)-0.48
r=1.0000
p=0.0028
238Uauth [dpm g-1]

Table 1: Position and sedimentology of the studied sediment samples. Grey shading indicates the core sites under slowly accumulating conditions.

	latitude	longitude	water depth [m]	sample depth [cm]	interpolated age BP [kyr]	DBD [g/cm³]	TOC [%]	$CaCO_3$ [%]	opal [%]
GeoB1027-2	-19.6558	9.1377	2668	13-16	3.1	0.76	0.64[a]	83[a]	n.a.
GeoB1028-4	-20.0993	9.1777	2215	16-19	4.8	0.80	0.28[b]	93[b]	0.5[b]
PS1768-8	-52.5930	4.4760	3299	166-169	16	0.82[c]	0.47[c] (1.03)[e]	0.9[c]	55
PS1769-1	-52.6125	4.4580	3269	14-16	16	0.85[d]	0.21[d] (0.53)[e]	0.6[d]	60

[a] and [b] from Müller (2003a, 2003b).
[c] and [d] unpublished data (personal communication G.Kuhn) averaged over depth intervals 1.60-1.71m and 0.1-0.2m, respectively.
[e] TOC analyzed on size fraction <20µm

Table 2: Recovery and loss through the fractionation process. The recovery of sediment, Th and U after sieving and settling and the leaching loss of Th and U to the supernatant are given in % relative to initial bulk values. Grey shading indicates the core sites under more slowly accumulating conditions.

	recovery [%]				loss to supernatant [%]		
	sediment after fractionation	^{230}Th	^{232}Th	^{238}U	^{230}Th	^{232}Th	^{238}U
GeoB1027-2 pureW	93	104	106	94	0.3	0.6	20.7
GeoB1027-2 seaW	100	94	95	n.a.	0.8	0.5	n.a.
GeoB1028-4 pureW	94	99	100	59	0.3	0.5	17.1
GeoB1028-4 seaW	99	92	92	n.a.	1	0.7	n.a.
PS1768-8 pureW	81	87	82	96	3.1	1.7	36.6
PS1768-8 seaW	93	87	87	75	2.4	1.7	12.6
PS1769-1 pureW	86	86	85	100	1.1	0.6	8.6
PS1769-1 seaW	93	90	90	123	2.4	1.6	28.3

Table 3: Contribution of Th and U isotopes by each grain size class in percentage of the total inventory. Grey shading indicates the core sites under more slowly accumulating conditions. Errors are given as ±2σ.

	$^{230}Th_{xs}$ [%]				^{232}Th [%]				^{238}U [%]			
	GeoB1027	*GeoB1028*	*PS1768*	*PS1769*	*GeoB1027*	*GeoB1028*	*PS1768*	*PS1769*	*GeoB1027*	*GeoB1028*	*PS1768*	*PS1769*
<2µm pureW	53.1 ± 3.8	55.2 ± 5.0	88.7 ± 6.2	79.9 ± 5.7	59.1 ± 3.7	59.4 ± 3.1	69.2 ± 4.6	67.1 ± 4.5	57.7 ± 2.2	26.0 ± 1.0	72.6 ± 2.8	64.1 ± 2.4
2-20µm pureW	22.8 ± 1.4	11.7 ± 0.7	9.3 ± 0.6	15.3 ± 1.0	27.7 ± 0.9	17.4 ± 0.5	26.5 ± 0.9	25.1 ± 0.9	18.6 ± 0.7	18.6 ± 0.7	22.5 ± 0.9	28.2 ± 1.1
20-63µm pureW	11.6 ± 0.7	6.3 ± 0.4	1.3 ± 0.1	2.7 ± 0.2	5.8 ± 0.2	3.9 ± 0.1	2.4 ± 0.1	3.9 ± 0.2	10.4 ± 0.4	8.9 ± 0.3	4.1 ± 0.2	5.6 ± 0.3
63-125µm pureW	6.8 ± 0.4	9.8 ± 0.6	0.3 ± 0.0	0.5 ± 0.1	3.6 ± 0.1	6.2 ± 0.2	1.1 ± 0.1	1.2 ± 0.1	6.8 ± 0.3	15.4 ± 0.6	0.4 ± 0.02	0.8 ± 0.0
>125µm pureW	5.6 ± 0.4	16.9 ± 1.0	0.4 ± 0.1	1.5 ± 0.1	3.9 ± 0.1	13.1 ± 0.4	0.9 ± 0.0	2.7 ± 0.1	6.5 ± 0.2	31.1 ± 1.2	0.4 ± 0.02	1.4 ± 0.1
<10µm seaW	54.0 ± 3.9	50.2 ± 3.6	88.9 ± 6.4	88.4 ± 6.7	66.2 ± 3.7	58.3 ± 2.6	88.8 ± 4.0	86.9 ± 4.8	47.8 ± 1.8	35.8 ± 1.4	89.1 ± 3.6	85.5 ± 3.4
10-20µm seaW	5.9 ± 0.4	2.9 ± 0.2	1.4 ± 0.1	1.1 ± 0.1	6.1 ± 0.2	3.3 ± 0.1	2.7 ± 0.1	2.0 ± 0.1	4.7 ± 0.2	2.2 ± 0.1	1.1 ± 0.04	1.1 ± 0.0
20-63µm seaW	11.0 ± 0.7	7.6 ± 0.5	7.7 ± 0.7	7.2 ± 0.6	6.8 ± 0.2	4.9 ± 0.2	6.5 ± 0.3	6.7 ± 0.3	11.3 ± 0.4	7.7 ± 0.3	8.0 ± 0.4	10.2 ± 0.6
63-125µm seaW	10.5 ± 0.6	11.5 ± 0.7	1.4 ± 0.1	1.6 ± 0.2	6.6 ± 0.2	8.1 ± 0.3	1.1 ± 0.1	1.8 ± 0.1	12.1 ± 0.5	12.8 ± 0.5	1.4 ± 0.1	1.7 ± 0.1
>125µm seaW	18.6 ± 1.1	27.8 ± 1.7	0.6 ± 0.1	1.7 ± 0.2	14.2 ± 0.4	25.4 ± 0.8	0.9 ± 0.1	2.6 ± 0.1	24.0 ± 1.0	41.4 ± 1.6	0.4 ± 0.02	1.5 ± 0.1

Table 4: Characterization of the particle fractions obtained by sieving and settling. The analyses of specific surface area and grain size and the SEM imaging have been performed on the size fractions of GeoB1027 and PS1769. Biogenic opal has been analyzed on fractions of the opal-rich sediment (more opal data in Table A1, appendix A). "f" and "s" mean fast settling and slowly settling, respectively.

	specific surface area [m²/g]	mean grain size [µm]	biogenic opal [%]	particle composition (minor components are in parantheses)
GeoB1027-2				
bulk	9.2	29.3	n.a.	
<2µm	29.1	2.3	n.a.	clay + coccoliths
2-20µm	5.7	6.4	n.a.	coccoliths + foraminifera fragments
20-63µm	5.2	33.7	n.a.	foraminifera and foram. fragments
63-125µm	4.3	79.6	n.a.	foraminifera
>125µm	4.3	204.1	n.a.	foraminifera
PS1769-1				
bulk	19.2	22.3	60	
<2µm	56.5	2.6	61	clay + diatom fragments
2-20µm	13.0	10.9	80	diatom fragments
f 20-63µm	2.7	41.4	17	rock fragments (+ radiolarians + diatoms)
f 63-125µm	1.6	87.0	5	rock fragments + radiolarians
f >125µm	3.3	418.1	4	rock fragments + radiolarians
s 20-63µm	11.2	30.4	82	diatoms
s 63-125µm	9.5	70.4	79	diatoms
s >125µm	n.a.	154.2	n.a.	diatoms (+ radiolarians)

Table 5: Estimation of grain size sorting effects on focusing factor (Ψ) and $^{230}Th_{xs}$ normalized vertical flux (F_V). Ψ and F_V are corrected for selective depositions of grain sizes <125µm, <63µm and <10µm (seaW fractions). In contrast the mass accumulation rate (MAR) show the uncorrected sediment flux to the seafloor.

	Ψ corrected for the deposition of				F_V [g/cm²/kyr] corrected for the deposition of				MAR [g/cm²/kyr]
	bulk	<125µm	<63µm	<10µm	bulk	<125µm	<63µm	<10µm	
GeoB1027-2	2.3	2.0	1.9	1.8	1.5	1.7	1.8	1.9	3.4
GeoB1028-4	1.8	1.5	1.4	1.3	1.7	2.1	2.2	2.4	3.0
PS1768-8	5.9	5.5	5.0	3.2	1.7	1.8	2.0	3.1	10.1
PS1769-1	3.2	3.0	2.8	2.1	1.4	1.5	1.6	2.1	4.4

Appendix A – Supplementary Data

Table A1: Opal content and concentrations of some elements in particle fractions of the samples PS1768-8 and PS1769-1.

sediment core (sample depth)	fractionation method	particle size class [µm]	settling velocity	biogenic opal [%]	Mg [%]	sd [%]	Al [%]	sd [%]	K [%]	sd [%]	Ca [%]	sd [%]	Mn [g/kg]	sd [%]	Fe [%]	sd [%]	Rb [ppm]	sd [%]	Cs [ppm]	sd [%]
PS1768-8 (166-169cm)	bulk			55	0.99	1.6	2.03	1.5	0.69	0.7	0.73	1.3	0.20	0.4	1.36	0.5	23.8	1.8	1.80	1.8
	pureW	<2		68	0.72	1.5	2.37	1.5	0.61	2.1	0.33	1.8	0.16	0.7	1.45	1.2	29.8	2.3	2.55	1.7
	pureW	2-20		76	0.22	1.6	1.38	1.1	0.41	0.5	0.61	0.6	0.11	1.3	0.67	0.8	9.9	0.7	0.69	1.3
	pureW	20-63	fast	n.a.	1.49	2.9	6.33	1.2	0.49	0.6	7.42	0.7	1.01	1.3	5.12	1.6	14.6	0.5	0.70	1.0
	pureW	63-125	fast	n.a.	1.91	2.8	7.31	1.7	0.61	0.2	7.09	2.2	1.11	2.1	5.60	1.0	12.7	0.8	0.80	0.6
	pureW	>125	fast	n.a.	2.29	0.2	7.38	1.2	0.48	1.0	8.34	1.3	1.12	1.3	5.67	2.6	10.0	0.4	0.62	0.7
	pureW	20-63	slowly	n.a.	0.04	1.7	0.17	0.9	0.10	0.2	0.12	2.2	0.02	0.9	0.07	0.6	1.1	0.8	0.16	0.6
	pureW	63-125	slowly	n.a.	0.06	1.5	0.21	1.6	0.08	1.8	0.24	1.0	0.03	1.0	0.14	1.0	2.0	0.6	1.11	0.2
	pureW	>125	slowly	n.a.	0.19	1.8	0.88	0.9	0.18	1.1	0.72	0.5	0.14	1.4	0.75	1.0	3.9	0.8	0.88	0.6
	seaW	<10		60	0.68	2.8	1.98	0.5	0.95	1.6	0.52	0.9	0.14	0.0	1.23	0.0	23.6	0.4	1.80	1.4
	seaW	10-20		n.a.	1.06	0.9	4.97	0.9	0.97	0.9	3.80	0.6	0.60	1.6	3.90	0.2	21.4	0.5	1.21	0.5
	seaW	20-63	fast	15	1.34	1.2	5.81	2.0	0.70	2.1	5.25	0.2	0.84	3.4	4.62	1.1	13.6	0.9	0.68	0.6
	seaW	63-125	fast	n.a.	2.01	1.9	7.30	2.5	0.47	1.8	7.23	3.0	1.13	1.1	6.01	0.6	14.2	0.8	0.69	0.7
	seaW	>125	fast	3	1.78	0.9	6.17	1.4	0.43	2.4	5.25	0.5	0.98	1.0	4.87	1.6	13.7	1.6	0.82	1.2
	seaW	20-63	slowly	75	0.27	1.5	0.57	2.9	0.29	2.7	0.28	0.5	0.06	0.7	0.39	4.8	5.5	1.2	0.45	0.7
	seaW	63-125	slowly	76	0.16	0.9	0.42	1.4	0.14	1.8	0.23	0.8	0.05	3.0	0.31	1.3	3.9	0.3	0.36	1.0
	seaW	>125	slowly	n.a.	0.32	3.7	0.95	1.3	0.21	2.2	1.76	0.1	0.16	0.5	0.88	0.8	7.2	0.4	0.87	0.7
PS1769-1 (14-16cm)	bulk			60	0.95	2.2	1.97	1.7	0.91	1.5	1.13	1.7	0.44	1.6	1.68	1.7	19.5	1.2	1.36	0.4
	pureW	<2		61	0.79	0.2	2.31	1.3	0.58	1.1	0.19	1.1	0.33	0.7	2.05	0.4	29.1	0.6	2.40	2.7
	pureW	2-20		80	0.20	1.7	1.17	1.1	0.38	0.5	0.58	1.4	0.28	1.2	0.63	1.3	8.5	0.5	0.52	0.8
	pureW	20-63	fast	n.a.	1.45	0.8	5.92	1.2	0.87	2.3	6.04	0.6	0.99	2.2	4.68	0.9	16.2	1.2	0.67	0.7
	pureW	63-125	fast	n.a.	2.05	2.8	7.47	0.7	0.66	1.7	7.43	0.9	1.17	0.7	5.98	1.3	13.1	1.2	0.67	1.2
	pureW	>125	fast	n.a.	3.08	1.2	7.31	1.8	0.62	1.4	6.88	0.3	1.18	0.2	6.26	1.1	11.9	0.6	0.59	0.9
	pureW	20-63	slowly	n.a.	0.04	1.8	0.21	1.6	0.12	1.5	0.19	1.3	0.15	0.7	0.12	0.4	1.2	0.6	0.11	1.5
	pureW	63-125	slowly	n.a.	0.06	1.0	0.29	0.6	0.12	0.8	0.27	2.2	0.19	1.3	0.20	1.4	1.7	0.8	0.44	0.3
	pureW	>125	slowly	n.a.	0.30	0.7	1.10	1.0	0.25	1.4	1.31	0.9	0.28	0.5	1.06	1.0	5.8	1.3	0.55	1.3
	seaW	<10		59	0.74	1.5	1.71	0.5	0.63	0.3	0.55	2.2	0.30	1.3	1.47	1.9	22.8	0.5	1.59	0.4
	seaW	10-20		n.a.	1.10	1.7	4.85	1.2	0.81	0.6	3.74	1.4	0.77	0.7	3.59	1.8	25.1	2.0	1.04	1.1
	seaW	20-63	fast	17	1.45	1.5	5.65	1.9	0.60	3.0	5.20	2.5	1.01	0.3	4.83	0.7	17.1	0.7	0.66	0.5
	seaW	63-125	fast	5	1.93	0.2	6.96	1.2	0.48	0.5	6.90	1.4	1.16	0.4	5.77	0.0	14.5	0.2	0.69	0.8
	seaW	>125	fast	4	2.06	1.8	6.86	0.5	0.43	1.6	6.10	1.6	1.32	0.9	6.41	0.7	14.1	1.0	0.79	0.8
	seaW	20-63	slowly	82	0.22	1.5	0.35	1.3	0.17	1.7	0.17	1.4	0.23	0.4	0.28	1.7	3.5	1.3	0.25	0.3
	seaW	63-125	slowly	79	0.19	0.5	0.48	0.6	0.14	1.9	0.33	2.2	0.36	0.9	0.42	0.8	3.1	0.2	0.26	0.5
	seaW	>125	slowly	n.a.	0.27	0.7	0.78	0.2	0.23	1.2	0.98	1.9	0.31	0.3	0.94	0.4	8.8	0.1	0.75	0.6

Table A2: Th and U specific activities in particle fractions of the carbonate and the siliceous samples.

sediment core (sample depth)	fractionation method	particle size class [µm]	settling velocity	size fraction	230Th	2σ	230Th-xs	2σ	232Th	2σ	234U	2σ	235U	2σ	238U-total	2σ	238U-auth	2σ	auth. U in % of total U	234U/238U	2σ
				[%]	[dpm g^{-1}]																
GeoB1027-2 (13-16cm)	bulk				5.0	0.2	4.7	1.6	0.56	0.02	2.35	0.09	0.095	0.004	2.07	0.08	1.73	0.58	84	1.13	0.06
	pureW	<2		35.2	7.9	0.3	7.4	2.5	0.99	0.03	2.84	0.11	0.116	0.004	2.51	0.10	1.92	0.64	76	1.13	0.06
	pureW	2-20		27.5	4.3	0.1	4.0	1.4	0.60	0.02	1.12	0.04	0.047	0.002	1.01	0.04	0.65	0.22	65	1.11	0.06
	pureW	20-63		15.9	3.6	0.1	3.6	1.2	0.22	0.01	1.15	0.05	0.045	0.002	0.98	0.04	0.85	0.28	87	1.18	0.07
	pureW	63-125		11.1	3.1	0.1	3.0	1.0	0.19	0.01	1.08	0.04	0.042	0.002	0.92	0.04	0.80	0.27	87	1.18	0.06
	pureW	>125		10.3	2.7	0.1	2.7	0.9	0.22	0.01	1.07	0.04	0.043	0.002	0.94	0.04	0.81	0.27	86	1.14	0.06
	seaW	<10		43.4	5.8	0.2	5.5	1.8	0.80	0.03	1.51	0.06	0.061	0.002	1.33	0.05	0.85	0.28	64	1.14	0.06
	seaW	10-20		5.9	4.7	0.2	4.4	1.5	0.56	0.02	1.10	0.04	0.045	0.002	0.97	0.04	0.64	0.21	66	1.13	0.06
	seaW	20-63		11.2	4.4	0.2	4.3	1.5	0.32	0.01	1.43	0.06	0.056	0.002	1.22	0.05	1.03	0.34	84	1.17	0.06
	seaW	63-125		12.9	3.7	0.1	3.6	1.2	0.27	0.01	1.33	0.05	0.052	0.002	1.13	0.04	0.97	0.32	85	1.18	0.06
	seaW	>125		26.7	3.2	0.1	3.1	1.0	0.28	0.01	1.26	0.05	0.050	0.002	1.08	0.04	0.92	0.31	84	1.17	0.07
GeoB1028-4 (16-19cm)	bulk				3.5	0.2	3.4	1.2	0.30	0.01	1.98	0.08	0.080	0.003	1.73	0.07	1.55	0.52	90	1.14	0.06
	pureW	<2		25.0	7.7	0.3	7.6	2.6	0.70	0.02	0.84	0.04	0.035	0.001	0.76	0.03	0.33	0.11	44	1.11	0.06
	pureW	2-20		12.6	3.3	0.1	3.2	1.1	0.41	0.01	1.20	0.05	0.048	0.002	1.05	0.04	0.80	0.27	76	1.15	0.06
	pureW	20-63		9.1	2.4	0.1	2.4	0.8	0.13	0.00	0.83	0.03	0.032	0.001	0.70	0.03	0.62	0.21	89	1.19	0.07
	pureW	63-125		17.5	1.9	0.1	1.9	0.6	0.11	0.00	0.74	0.03	0.029	0.001	0.63	0.02	0.56	0.19	90	1.18	0.06
	pureW	>125		35.9	1.6	0.1	1.6	0.5	0.11	0.00	0.73	0.03	0.028	0.001	0.62	0.02	0.55	0.18	89	1.18	0.06
	seaW	<10		28.3	5.7	0.2	5.6	1.9	0.57	0.02	1.29	0.05	0.052	0.002	1.12	0.04	0.78	0.26	70	1.15	0.06
	seaW	10-20		3.0	3.1	0.1	3.0	1.0	0.30	0.01	0.75	0.03	0.030	0.001	0.64	0.03	0.46	0.16	72	1.16	0.06
	seaW	20-63		9.1	2.6	0.1	2.6	0.9	0.15	0.00	0.88	0.03	0.034	0.001	0.74	0.03	0.66	0.22	88	1.18	0.06
	seaW	63-125		17.3	2.1	0.1	2.1	0.7	0.13	0.00	0.77	0.03	0.030	0.001	0.65	0.03	0.57	0.19	88	1.18	0.06
	seaW	>125		42.3	2.1	0.1	2.1	0.7	0.17	0.01	1.00	0.04	0.040	0.002	0.86	0.03	0.76	0.26	88	1.17	0.06
PS1768-8 (166-169cm)	bulk				6.5	0.2	6.6	2.2	0.52	0.02	3.40	0.13	0.140	0.005	3.04	0.12	2.73	0.92	90	1.12	0.06
	pureW	<2		39.6	11.9	0.4	12.7	2.4	0.84	0.03	4.47	0.17	0.181	0.007	3.04	0.12	2.67	1.19	88	1.14	0.06
	pureW	2-20		43.6	1.3	0.1	1.2	0.4	0.26	0.01	0.90	0.04	0.037	0.001	0.80	0.03	0.65	0.22	81	1.11	0.06
	pureW	20-63	fast	2.4	1.6	0.1	1.6	0.5	0.34	0.01	0.54	0.03	0.022	0.001	0.48	0.02	0.28	0.09	58	1.12	0.07
	pureW	63-125	fast	1.0	1.1	0.1	1.1	0.4	0.21	0.01	0.38	0.02	0.016	0.001	0.35	0.01	0.22	0.07	64	1.08	0.07
	pureW	>125	fast	1.8	1.1	0.0	1.1	0.4	0.19	0.01	0.33	0.02	0.014	0.001	0.30	0.01	0.19	0.06	61	1.09	0.07
	pureW	20-63	slowly	10.8	0.4	0.0	0.3	0.1	0.02	0.00	0.56	0.02	0.022	0.001	0.49	0.02	0.48	0.16	98	1.15	0.07
	pureW	63-125	slowly	0.6	1.4	0.1	1.3	0.5	0.43	0.01	0.35	0.02	0.016	0.001	0.34	0.01	0.09	0.03	26	1.02	0.08
	pureW	>125	slowly	0.2	0.7	0.1	0.7	0.2	0.08	0.00	0.42	0.03	0.017	0.001	0.38	0.01	0.33	0.11	88	1.10	0.09
	seaW	<10		74.1	6.6	0.2	7.0	2.3	0.54	0.02	2.56	0.10	0.104	0.004	2.27	0.09	1.95	0.65	86	1.13	0.06
	seaW	10-20		1.8	4.3	0.2	4.4	1.5	0.66	0.03	1.25	0.05	0.052	0.002	1.13	0.04	0.73	0.25	65	1.10	0.06
	seaW	20-63	fast	2.2	2.9	0.1	3.1	1.1	0.31	0.01	0.68	0.04	0.028	0.001	0.61	0.02	0.42	0.14	70	1.12	0.08
	seaW	63-125	fast	0.9	2.5	0.1	2.7	0.9	0.24	0.01	0.47	0.02	0.019	0.001	0.41	0.02	0.26	0.09	64	1.14	0.06
	seaW	>125	fast	1.9	1.4	0.1	1.4	0.5	0.18	0.01	0.41	0.02	0.017	0.001	0.36	0.01	0.25	0.08	70	1.14	0.07
	seaW	20-63	slowly	16.0	2.2	0.1	2.3	0.8	0.14	0.00	0.99	0.05	0.039	0.002	0.85	0.03	0.76	0.26	90	1.17	0.07
	seaW	63-125	slowly	2.7	2.0	0.1	2.1	0.7	0.11	0.00	0.93	0.04	0.037	0.001	0.80	0.03	0.74	0.25	92	1.16	0.06
	seaW	>125	slowly	0.2	3.8	0.2	4.2	1.4	0.22	0.01	0.77	0.06	0.030	0.001	0.66	0.03	0.53	0.18	80	1.17	0.10
PS1769-1 (14-16cm)	bulk				6.1	0.2	6.7	2.2	0.46	0.02	0.72	0.03	0.030	0.001	0.66	0.03	0.38	0.13	58	1.09	0.06
	pureW	<2		35.5	11.5	0.4	12.7	3.9	0.76	0.02	1.19	0.05	0.053	0.002	1.08	0.04	0.65	0.24	60	1.04	0.06
	pureW	2-20		40.6	2.0	0.1	2.1	0.7	0.24	0.01	0.45	0.02	0.019	0.001	0.41	0.02	0.27	0.09	65	1.10	0.06
	pureW	20-63	fast	2.1	2.7	0.1	2.8	0.9	0.52	0.02	0.43	0.02	0.020	0.001	0.43	0.02	0.12	0.04	27	1.02	0.06
	pureW	63-125	fast	1.8	1.5	0.1	1.6	0.5	0.25	0.01	0.20	0.01	0.009	0.000	0.20	0.01	0.05	0.02	25	1.00	0.06
	pureW	>125	fast	4.6	1.4	0.1	1.5	0.5	0.20	0.01	0.16	0.01	0.007	0.000	0.16	0.01	0.04	0.01	23	1.01	0.06
	pureW	20-63	slowly	14.1	0.6	0.0	0.7	0.2	0.03	0.00	0.19	0.01	0.008	0.000	0.17	0.01	0.15	0.05	89	1.12	0.07
	pureW	63-125	slowly	0.6	0.5	0.0	0.5	0.2	0.03	0.00	0.16	0.01	0.007	0.000	0.15	0.01	0.13	0.04	87	1.06	0.07
	pureW	>125	slowly	0.6	2.4	0.1	2.6	0.9	0.16	0.01	0.14	0.01	0.007	0.000	0.14	0.01	0.05	0.02	33	0.99	0.08
	seaW	<10		68.1	7.0	0.3	7.7	2.6	0.52	0.02	0.86	0.03	0.036	0.001	0.79	0.03	0.47	0.16	60	1.09	0.06
	seaW	10-20		1.0	6.0	0.2	6.4	2.1	0.85	0.03	0.72	0.03	0.031	0.001	0.68	0.03	0.17	0.06	25	1.05	0.06
	seaW	20-63	fast	1.8	3.9	0.1	4.2	1.4	0.51	0.02	0.46	0.02	0.021	0.001	0.45	0.02	0.14	0.05	32	1.03	0.06
	seaW	63-125	fast	1.6	2.3	0.1	2.5	0.8	0.30	0.01	0.24	0.01	0.010	0.000	0.23	0.01	0.05	0.02	22	1.05	0.06
	seaW	>125	fast	4.1	1.9	0.1	2.0	0.7	0.23	0.01	0.21	0.01	0.009	0.000	0.20	0.01	0.06	0.02	32	1.04	0.06
	seaW	20-63	slowly	20.3	1.6	0.1	1.7	0.6	0.09	0.00	0.31	0.02	0.013	0.001	0.27	0.01	0.22	0.07	80	1.15	0.07
	seaW	63-125	slowly	2.7	1.8	0.1	2.0	0.7	0.10	0.00	0.29	0.01	0.012	0.000	0.26	0.01	0.20	0.07	78	1.13	0.07
	seaW	>125	slowly	0.5	3.4	0.1	3.8	1.3	0.21	0.01	0.21	0.01	0.009	0.000	0.20	0.01	0.07	0.02	36	1.05	0.07

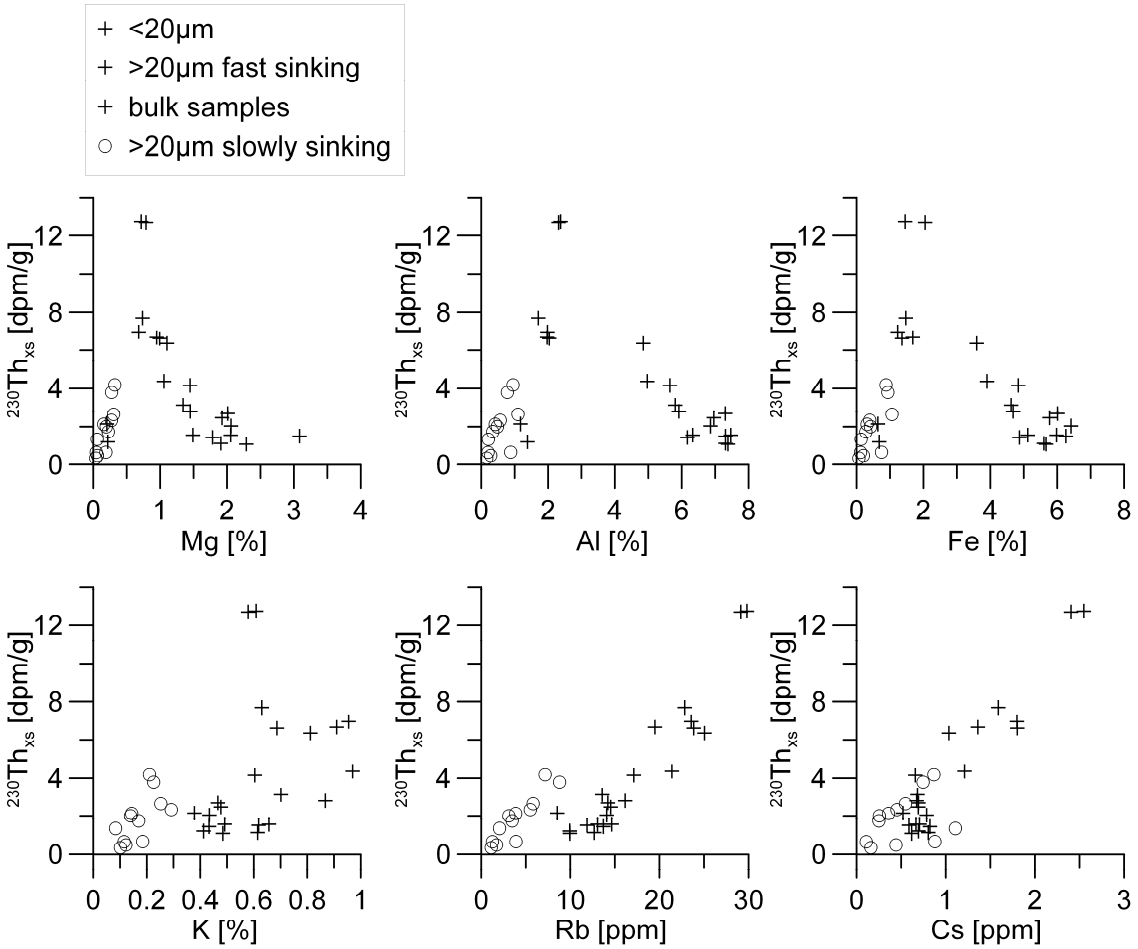

Figure A1: Scatter plot of $^{230}Th_{xs}$ specific activities against different element concentrations within the sediment fractions of the samples from cores PS1768-8 and PS1769-1. The particle class >20µm (slowly sinking) is depicted as a circle (○) and all other particle classes are depicted as a cross (+). Only Rb and Cs show positive correlations with $^{230}Th_{xs}$.

Appendix B – Derivation of the equation for calculating a grain size corrected focusing factor

Measured composition

i	grain size fraction measured in sediment
T_i	$^{230}Th_{xs}$ activity [dpm/g] in grain size fraction i
T_m	$^{230}Th_{xs}$ activity [dpm/g] in bulk sample
k_m	portion of small particles measured in sediment
Ψ	focusing factor measured

The $^{230}Th_{xs}$ activity T in the fraction of small (or large) sized particles is calculated as the sum of the grain size weighted $^{230}Th_{xs}$ activities.

$$T = \sum (T_i \times i)$$

We can calculate the variables for the lateral (vertical) composition for any choice of the grain size distribution in the lateral (vertical) flux.

T_{kL}	$^{230}Th_{xs}$ activity in small particles in lateral flux
T_{gL}	$^{230}Th_{xs}$ activity in large particles in lateral flux
T_{kV}	$^{230}Th_{xs}$ activity in small particles in vertical flux
T_{gV}	$^{230}Th_{xs}$ activity in large particles in vertical flux
k_L	portion of small particles in the lateral flux

Calculation

x	portion of the lateral flux related to the sedimentation rate
k_V	portion of small particles in vertical flux

With those variables as defined above, there are two unknown variables to be solved by two equations. The first equation describes the composition of small particles by the lateral and the vertical contribution:

$$k_m = x\, k_L + (1–x)\, k_V \qquad (1)$$

so that the vertical contribution of small particles is:

$$k_V = \frac{k_m - x k_L}{1 - x} \qquad (2)$$

Equation (3) is calculating the focusing factor Ψ what is the total Th flux (vertical + lateral) divided by the vertical Th flux:

$$\Psi = \frac{x\left(k_L T_{kL} + (1-k_L) T_{gL}\right) + (1-x)\left(k_V T_{kV} + (1-k_V) T_{gV}\right)}{(1-x)\left(k_V T_{kV} + (1-k_V) T_{gV}\right)} \qquad (3)$$

This can be written as equation (4):

$$x\left(k_L T_{kL} + (1-k_L) T_{gL}\right) + (1-x) \times \left(k_V T_{kV} + (1-k_V) T_{gV}\right) = \Psi\left[(1-x)\left(k_V T_{kV} + (1-k_V) T_{gV}\right)\right] \qquad (4)$$

By substitution of k_V with equation (2) we obtain equation (5):

$$x\left(k_L T_{kL} + (1-k_L)T_{gL}\right) + \left(k_m - xk_L\right)\left(T_{kV} - T_{gV}\right) + T_{gV}(1-x) = \Psi\left[\left(k_m - xk_L\right)\left(T_{kV} - T_{gV}\right) + T_{gV}(1-x)\right] \quad (5)$$

Which is simplified and solved for x:

$$x = \frac{(\Psi - 1)\left(k_m\left(T_{kV} - T_{gV}\right)\right) + T_{gV}}{k_L T_{kL} + (1-k_L)T_{gL} + (\Psi - 1)\left(k_L\left(T_{kV} - T_{gV}\right) + T_{gV}\right)} \quad (6)$$

If the portion of fine particles in the lateral flux is 100% we can set:

$k_L = 1$ (7)

As Th activities in vertical and lateral fluxes are unknown we assume same activities for both fluxes. Than we can write:

$T_{kV} = T_{kL}$, simply T_k (8)

and

$T_{gV} = T_{gL}$, simply T_g (9)

With the assumptions (7-9) the equation can be simplified written as:

$$x = \frac{(\Psi - 1)\left(k_m T_k + (1-k_m)T_g\right)}{\Psi T_k} \quad (10)$$

This is the same as

$$x = \frac{(\Psi - 1)T_m}{\Psi T_k} = \frac{T_m}{T_k}\left(1 - \frac{1}{\Psi}\right) \quad (11)$$

Knowing the portion of lateral flux (x) and vertical flux (1-x) we are able to calculate the grain size corrected focusing factor Ψ_c:

$$\Psi_c = \frac{1}{1-x} = \frac{1}{1 - \frac{T_m}{T_k}\left(1 - \frac{1}{\Psi}\right)} \quad (12)$$